Geol. Mag. **156** (*5*), *2019, pp. 811–832* © *Cambridge University Press 2018*
doi:10.1017/S0016756818000183

Superimposed deformation of the Solonker Belt and nearby regions in western Inner Mongolia, China

GUANZHONG SHI*‡, CHAO LIANG*‡, HUA WANG*‡† & CHUANYAN HUANG*‡

*Key Laboratory of Tectonics and Petroleum Resources, Ministry of Education, China University of Geosciences, Wuhan 430074, China
‡Faculty of Earth Resources, China University of Geosciences, Wuhan 430074, China

(*Received* 12 November 2017; *accepted* 13 February 2018; *first published online* 10 April 2018)

Abstract – The deformation of the Solonker Belt and nearby regions is helpful for understanding the tectonic evolution of the Central Asian Orogenic Belt. This study carried out structural analysis in the Mandula and Ganqi areas of western Inner Mongolia, including the Solonker Belt, the Southern Orogenic Belt and the northern Yinshan Belt (Langshan range). Our results reveal that the Solonker Belt, the Southern Orogenic Belt and the northern Yinshan Belt underwent two stages (D1 and D2) of deformation during the Mesozoic period. The D1 stage produced the NNE-directed thrusts and asymmetric folds, indicating a NNE–SSW contraction. The northern Yinshan Belt, the Southern Orogenic Belt and the Solonker Belt formed as a series of NNE-verging tectonic nappes. The D2 stage developed the NE-trending folds and the SE- or NW-directed thrusts that cross-cut the D1 structures. The two events of nearly orthogonal or oblique shortening gave rise to the superimposed structures (e.g. fold interference patterns). The quartz veins that filled the fractures of the D1 deformation contain zircons of Middle Triassic U–Pb ages. The new dating data, along with the regional sedimentary hiatus, led us to infer that the D1 stage of deformation occurred in Middle Triassic time and the D2 stage occurred in Late Jurassic time. We consider that the D1 stage of deformation resulted from a convergent event, which might be related to the closure of the Palaeo-Asian Ocean or limited, narrow ocean basins; and the D2 stage of deformation was the far-field result of subduction of the Palaeo-Pacific Ocean and the closure of the Mongol-Okhotsk Ocean.

Keywords: structural analysis, Solonker Belt, Mesozoic, Central Asian Orogenic Belt, Inner Mongolia.

1. Introduction

The Central Asian Orogenic Belt (CAOB) is a giant tectonic collage between the Siberian Craton and North China–Tarim cratons (Sengör, Natal'in & Burtman, 1993; Jahn, 2004; Windley *et al.* 2007; Xiao *et al.* 2009, 2015). It was built up by multiple subduction/accretionary and collisional processes along with the closure of the Palaeo-Asian Ocean, and various tectonic units were involved, such as Precambrian microcontinents, ancient island arcs, fragments of oceanic islands and seamounts, accretionary complexes and passive continental margins (Mossakovsky *et al.* 1993; Sengör, Natal'in & Burtman, 1993; Jahn, 2004; Windley *et al.* 2007).

Many studies have been carried out to understand the tectonic processes of the CAOB, but the timing of the final closure of the Palaeo-Asian Ocean is highly controversial, ranging from Late Devonian to Triassic (Xiao *et al.* 2003; Lin *et al.* 2008; Charvet *et al.* 2011; Xu *et al.* 2013; Eizenhöfer *et al.* 2014, 2015*a*,*b*; Shao, Tang & He, 2014; Li *et al.* 2014, 2017*a*,*b*,*c*; Liu *et al.* 2017). The Solonker Belt has been considered a Late Permian to Middle Triassic suture zone, with Early Palaeozoic subduction-accretionary rocks distributed to its north and south (Xiao *et al.* 2003, 2015; Li *et al.* 2014, 2017*b*,*c*; Eizenhöfer *et al.* 2015*a*,*b*; Liu *et al.* 2016). In contrast, some studies have regarded the Solonker Belt as a Permian extensional zone which was built on the Early Palaeozoic orogens (Chen *et al.* 2012; Xu *et al.* 2013; Shao, Tang & He, 2014; Luo *et al.* 2016; Wang, X. C. *et al.* 2016).

The Yinshan–Yanshan Belt is situated to the south of the CAOB and has undergone polyphase deformation during the Mesozoic period, which might have genetic links with: (i) the closure of the Palaeo-Asian Ocean at *c*. 250–200 Ma (e.g. Cui & Wu, 1997; Wang, Zhou & Li, 2011), (ii) the Jurassic closure of the Mongol-Okhotsk Ocean (Wang, Zhou & Li, 2011; Zhang, J. *et al.* 2014) or (iii) the westward indentation of the North China Plate due to the subduction of the Palaeo-Pacific Ocean (e.g. Faure, Lin & Chen, 2012).

Some studies have examined the sedimentary, volcanic and metamorphic history in/adjacent to the Solonker Belt (e.g. Chen *et al.* 2000; Xiao *et al.* 2003, 2015; Xu *et al.* 2013; Song *et al.* 2015; Eizenhöfer *et al.* 2015*a*,*b*; Zhang, Wei & Chu, 2015; Zhang *et al.* 2016), but the scarcity of structural analysis greatly limits our understanding of the tectonic development of the Solonker Belt. In order to unravel the genetic mechanism of the Solonker Belt and its

†Author for correspondence: wanghua@cug.edu.cn

corresponding tectonic events, this paper deals with the superimposed deformation of the Solonker Belt, the Southern Orogenic Belt and the northern Yinshan Belt exposed in western Inner Mongolia (Fig. 1). In the following, two main questions will be addressed, namely (i) what is the bulk geometry and kinematics deduced from the structural analysis? And (ii) what are the timings of the deformation and their relationships with the regional geodynamic events?

2. Geological setting

The CAOB in Inner Mongolia is subdivided into several ENE-trending tectonic units, from south to north: the Southern Orogenic Belt, the Solonker Belt and the Northern Orogenic Belt. Several amalgamated microcontinents, including the Hunshandake block, the South Mongolia Microcontinent and the southern margin of the Ergun block, have been proposed to account for the present architecture (Fig. 1b; Xiao *et al.* 2003, 2009; Xu *et al.* 2013).

The Southern Orogenic Belt is separated from the North China Craton by the Bayan Obo–Chifeng fault and extends at least for > 700 km from the Ganqi area in the west via Ondor Sum to the Chifeng area in the east (Fig. 1b). It is composed of the Ordovician to Lower Silurian Ondor Sum Group, which is predominantly composed of sericite quartz schists, chlorite-epidote schists, albite-chlorite-epidote schists and meta-basalts, and the Early Palaeozoic Bainaimiao arc magmatic rocks (De Jong *et al.* 2006; Jian *et al.* 2008, 2010; Xu *et al.* 2013; Shi *et al.* 2013). Late Palaeozoic magmatic rocks overprinted the Early Palaeozoic Bainaimiao arc rocks (Zhang, S.-H. *et al.* 2009*a*,*b*, 2014). The Solonker Belt extends from the Ganqi area to the Linxi area (Fig. 1b; Wang & Liu, 1986; Xiao *et al.* 2003, 2015) and is composed of Upper Palaeozoic limestones, turbidites, volcaniclastic rocks, mafic rocks and rare amounts of ultramafic bodies (Wang & Liu, 1986; Xiao *et al.* 2003). The volcanic rocks and equivalent intrusions in the Solonker Belt have age ranges of *c*. 310–250 Ma (e.g. Jian *et al.* 2010; Eizenhöfer *et al.* 2014). The North Orogenic Belt is defined by the lithological association of Lower Palaeozoic Baolidao arc plutons (e.g. Chen *et al.* 2000; Jian *et al.* 2008), mélange rocks and Devonian molasse sandstones (Xu *et al.* 2013).

The Yinshan–Yanshan Belt is an E–W-trending Mesozoic tectonic unit, 1000 km in length, in the north of the North China Craton. The basement rocks of the Yinshan–Yanshan Belt consist of Archaean and Palaeoproterozoic gneisses unconformably covered by Meso- to Neoproterozoic terrigenous clastic strata and carbonates (Kusky & Li, 2003; Zhao, Sun & Wilde, 2005; Faure *et al.* 2007; Kusky, Windley & Zhai, 2007). The basement rocks are unconformably overlain by Upper Palaeozoic and Mesozoic sedimentary rocks. Our study area occupies the northern Yinshan Belt, which is separated from the CAOB to the north by the Bayan Obo fault and bounded by the Ordos basin to the south (Fig. 1c; Zhang, J. *et al.* 2013, 2014; Hu *et al.* 2014). Below we will describe the lithology and structural feature of the Late Palaeozoic Solonker Belt (the Mandula area), the Early Palaeozoic Southern Orogenic Belt (the Ganqi area) and the northern Yinshan Belt (the Langshan range; Fig. 1c).

3. Geology and structural deformation

3.a. The Mandula area (the Solonker Belt)

3.a.1. Lithostratigraphy and magmatic rocks

The Mandula area mainly exposes the Upper Carboniferous to Permian sedimentary and magmatic rocks. The southern part of the Mandula area is dominated by limestones and sandstones ascribed to the Upper Carboniferous to Lower Permian Amushan Formation (C_2–P_1a). However, these limestones are olistoliths sedimented into a siltstone-greywacke matrix, and thus the rocks are considered to have formed an olistostrome in Early Permian time (Shi, 2013). The olistostrome is characterized by metre- to kilometre-sized blocks of limestone and sandstone. The long axis of the olistoliths mostly strikes NW–SE (Fig. 2). The Lower Permian Baotege Formation (P_1b) and a basaltic lava unit crop out to the north of the olistostrome. The Baotege Formation is composed of well-stratified turbidite and marlstone with intercalations of volcanic layers. The basaltic lava was dated at 274 Ma (Chen *et al.* 2012). In the north, the Lower–Middle Permian Dashizhai Formation ($P_{1\text{-}2}d$) is composed of basaltic andesite, rhyolite, tuff, sandstone and silty mudstone (Zhang *et al.* 2008; Shao, Tang & He, 2014). The Middle Permian Zhesi Formation (P_2z) comprises lenticular limestone, conglomerate, sandstone and mudstone with a mixed fauna of Boreal and Tethyan domains (NMBGMR, 1991; Wang, Wang & Li, 2004).

The Upper Palaeozoic sedimentary rocks in the Mandula area are unconformably covered by the Cretaceous sedimentary rocks comprising conglomerates and sandstones (Fig. 2).

3.b.2. Polyphase deformation

Our field observations show that the olistostrome geometrically overlies the lower basaltic lavas of 274 Ma. The olistostrome and the lavas northwards thrust upon the Lower Permian Baotege Formation (P_1b) along the F1 fault (Figs 2, 3 A–A′). The F1 fault is an ESE-striking and SW-dipping thrust with a sinistral component. Immediately south of the fault, the basalts developed striae with a nearly N–S direction (Fig. 4a). Immediately north of the fault, the turbidite exhibits a SW-dipping cleavage, and the relationship between the bed and cleavage indicates an asymmetric fold. Drag folds are locally observed along the fault, indicating NE-directed thrusting with a left lateral strike-slip component (Fig. 4b).

The Lower Permian Baotege Formation tectonically overlies the Middle Permian Zhesi Formation (P_2z) as

https://doi.org/10.1017/S0016756818000183 Published online by Cambridge University Press

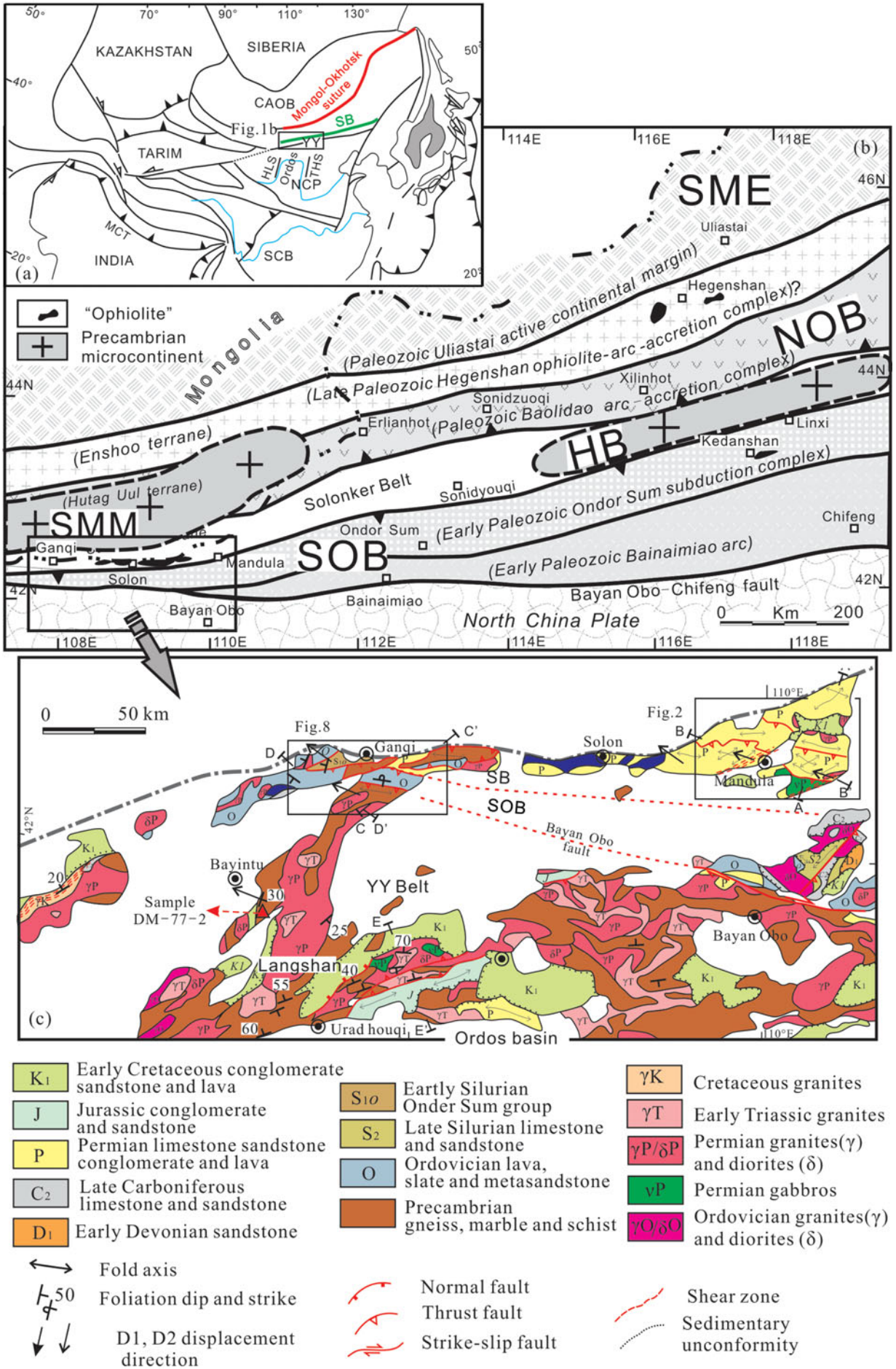

https://doi.org/10.1017/S0016756818000183 Published online by Cambridge University Press

a result of the F2 thrust fault. The F2 fault presents as geomorphologic valleys in the field, and the turbidite along the fault exhibits a WNW-trending cleavage. The Middle Permian Zhesi Formation develops open folds with predominant NE- or SW-dipping beds.

The F3 fault is a WNW–ESE-striking and NNE-directed thrust fault. It cross-cuts the Dashizhai Formation and results in the volcanic bodies forming pop-up structures along a SSW-directed antithetic thrust (Figs 2, 3 A–A′). The strata near the F3 fault are vertical and have developed a series of vertical, net-like joints.

The F4 fault developed in the sandstones of the Dashizhai Formation. The sandstones near the fault developed a vertical or NE-dipping cleavage. A sinistral strike-slip component is deduced from the drag folds in the sandstones.

There are small NE–SW-trending strike-slip faults in the Mandula area (Fig. 2), which dislocated the strata and accommodated the displacement of the abovementioned NNE-directed thrust faults.

The Mandula area also has two main NE–SW-trending, SE-dipping thrust faults, the F5 and F6 faults, which cross-cut the sedimentary formations and the Permian igneous plutons (Figs 2, 3 B–B′). The F5 thrust fault, 1–2 km in width, presents as an intensively cleaved zone in the basaltic lavas and a mylonitic zone in the granitic plutons and the limestones (P_2z) (Fig. 5a). Microscopic evidence in the mylonitic zone indicates a top-to-the-NW sense of shear (Fig. 5a, b). The F6 thrust fault, *c*. 1 km in width, cross-cuts the turbidite to produce the SE-dipping cleavage (Fig. 2). The striae on the F6 fault plane have a predominant NW–SE direction (Fig. 5c). Microscopic indicators of the F6 fault indicate a top-to-the-NW sense of displacement (Fig. 5d). In addition, NW- or SE-directed small thrust faults that cut the nearly WNW–ESE-trending folded strata are observed in places (Fig. 5e, f).

The strata in the Mandula area are intensively folded. The turbidite of the Baotege Formation has various dips (Figs 2, 6a, b). Two groups of shear joints and one group of E–W-trending tension joints are observed in the turbidite. In places, the joints are filled with white quartz veins (Fig. 4c). The volcanic beds of the Dashizhai Formation ($P_{1\text{-}2}d$) mostly dip to the north or south. By contrast, the volcaniclastic rocks have various dips and sometimes the strata are overturned (Fig. 6c). The sandstones of the Zhesi Formation have various dips, but mainly dip to the NW or SE when close to the F5 and F6 thrust faults (Fig. 2). In most cases, the sandstones developed a pervasive cleavage with a predominant WNW–ESE trend. But W-dipping cleavage is observed in places, and the relationship to the bed implies rotation by a later stage of deformation (Fig. 4d).

3.a.3. Interpretation

Our field observations indicate that the two NE–SW-trending, SE-dipping thrust faults (F5, F6) cross-cut the WNW–ESE-trending thrust faults (F1–F4; Table 1). Thus, two stages of deformation can be concluded. The D1 deformation is responsible for the development of the WNW–ESE-trending, NE- or NNE-directed thrust faults and the WNW–ESE-trending folds. Although the mineral stretching lineation cannot be seen in most cases, the cleavage can be recognized along the WNW–ESE-trending faulted zone, restricted to the areas near the faults, with predominant NNE or SSW dips (Fig. 2). The WNW–ESE-trending folds and the predominant NNE- or SSW-dipping cleavage in the faulted zones suggest the D1 stage of deformation is characterized by NNE–SSW contraction. The D2 deformation developed the NE–SW-trending, SE-dipping thrust faults and the NE–SW-trending folds, indicating a NW–SE contraction. The D2 deformation reworked the D1 folds and bent the fold axes (Fig. 2, see projection of intersection of bed and cleavage). Because of the superimposed deformation, the strata in the Mandula area are characterized by dome-and-basin or mega arrowhead-shaped structures (e.g. Ramsay & Huber, 1987; Deng, Koyi & Nilfouroushan, 2016), especially in the turbidite and fine-grained volcaniclastic rocks (Figs 6, 7).

3.b. The Ganqi area

3.b.1. Lithostratigraphy and magmatic rocks

The Ganqi area is mainly occupied by the Mesoproterozoic basement rocks, Ordovician arc-related meta-volcanic and meta-sedimentary rocks, the Ordovician to Silurian Ondor Sum Group composed of sericite quartz schist, iron-bearing quartzite and meta-volcanic rocks, and the Lower Permian Baotege Formation (Fig. 8). The Mesoproterozoic rocks in the southern Ganqi area are composed of gneiss, marble and meta-sedimentary rocks that were intruded by the Ordovician diorite and Permian granite (NMBGMR, 1991). The Ordovician meta-volcanic rocks mainly consist of basalt, andesite and dacite. The Ondor Sum Group has undergone greenschist-facies metamorphism and was interpreted as a subduction-related complex (Xu *et al.* 2013). The sericite quartz schist yielded a detrital zircon peak age of 444 Ma (Xu *et al.* 2016).

Figure 1. (Colour online) (a) The location of the study area in the eastern Eurasian continent. (b) Tectonic division of western and central Inner Mongolia (the tectonic division marked in italic is after Xiao *et al.* 2003 and Badarch, Cunningham & Windley, 2002; the tectonic division of the SOB and NOB, and the positions of the SME, SMM and HB are after Xu *et al.* 2013). (c) Geological map of the study area in western Inner Mongolia (after NMBGMR, 1991; Zhou *et al.* 2013). HLS – Helanshan; THS – Taihangshan; NCP – North China plate; SCB – South China Block; CAOB – Central Asian Orogenic Belt; SME – Southern Margin of the Ergun block; NOB – Northern Orogenic Belt; HB – Hunshandake block; SOB – Southern Orogenic Belt; SMM – Southern Mongolia Microcontinent; SB – Solonker Belt. YY – Yinshan–Yanshan Belt.

https://doi.org/10.1017/S0016756818000183 Published online by Cambridge University Press

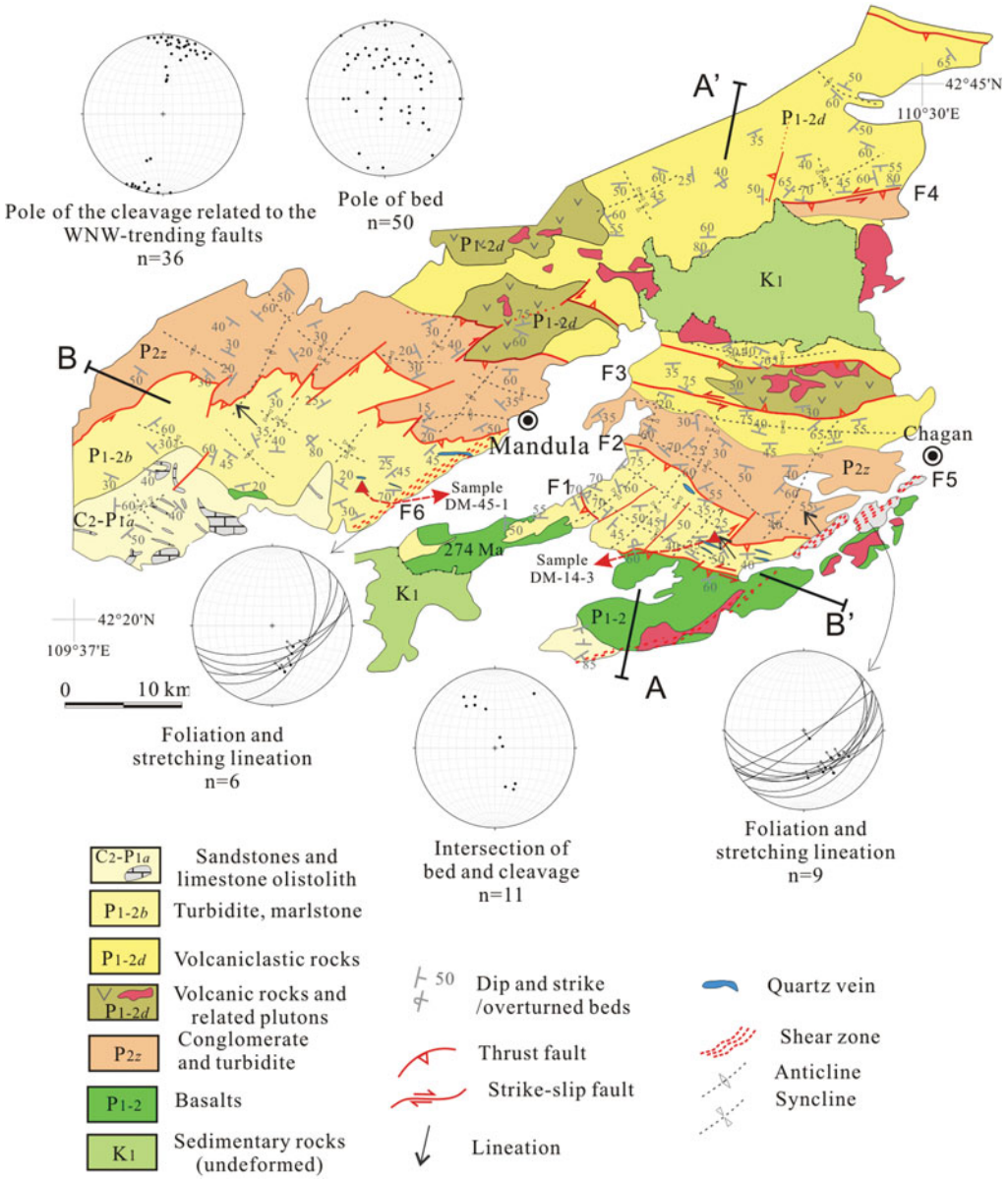

Figure 2. (Colour online) Geological and structural map of the Mandula area and lower hemisphere projections of the measured structural data.

The Ordovician to Silurian meta-volcanic rocks and subduction-related complex are defined as the Southern Orogenic Belt (Xu *et al.* 2013). The Baotege Formation in the Ganqi area is a succession of turbidites with intercalations of volcanic beds, which belong to the Solonker Belt.

3.b.2. *Polyphase deformation*

The Ganqi area has undergone a nearly N–S contraction due to the Early Palaeozoic orogeny (Xu *et al.* 2013). Here we choose the foliation as the reference surface (S_1) to the study the geological architecture. In places, the bedding of the meta-sedimentary rocks is consistent with the foliation ($S_{0\text{-}1}$).

From south to north, the Mesoproterozoic basement rocks, the Southern Orogenic Belt and the Solonker Belt formed as NNE-verging imbricated thrust nappes. The Mesoproterozoic basement rocks were thrust upon the Ordovician meta-volcanic rocks of the Southern Orogenic Belt through a NW–SE-striking and SW-dipping thrust (F7 fault, comparable to the Bayan Obo fault). Above the F7 fault, we observed a series of antithetic faults in the Mesoproterozoic amphibolites (Figs 3 C–C′, 9a). Immediately north of the F7 fault, the foliation of the Ordovician meta-volcanic rocks predominantly strikes WNW–ESE, nearly vertical, and the meta-volcanic rocks are characterized by NNE-verging tight isoclinal folds.

The Mesoproterozoic and Lower Palaeozoic rocks overthrust to the NNE upon the Permian volcaniclastic rocks to form a kilometre-scale klippe (Figs 3 C–C′, 9b). Moreover, the rocks in the klippe are overturned and intraformational folding is observed (Fig. 9c). The minimum distance between the klippe and the root zone is *c*. 15 km.

https://doi.org/10.1017/S0016756818000183 Published online by Cambridge University Press

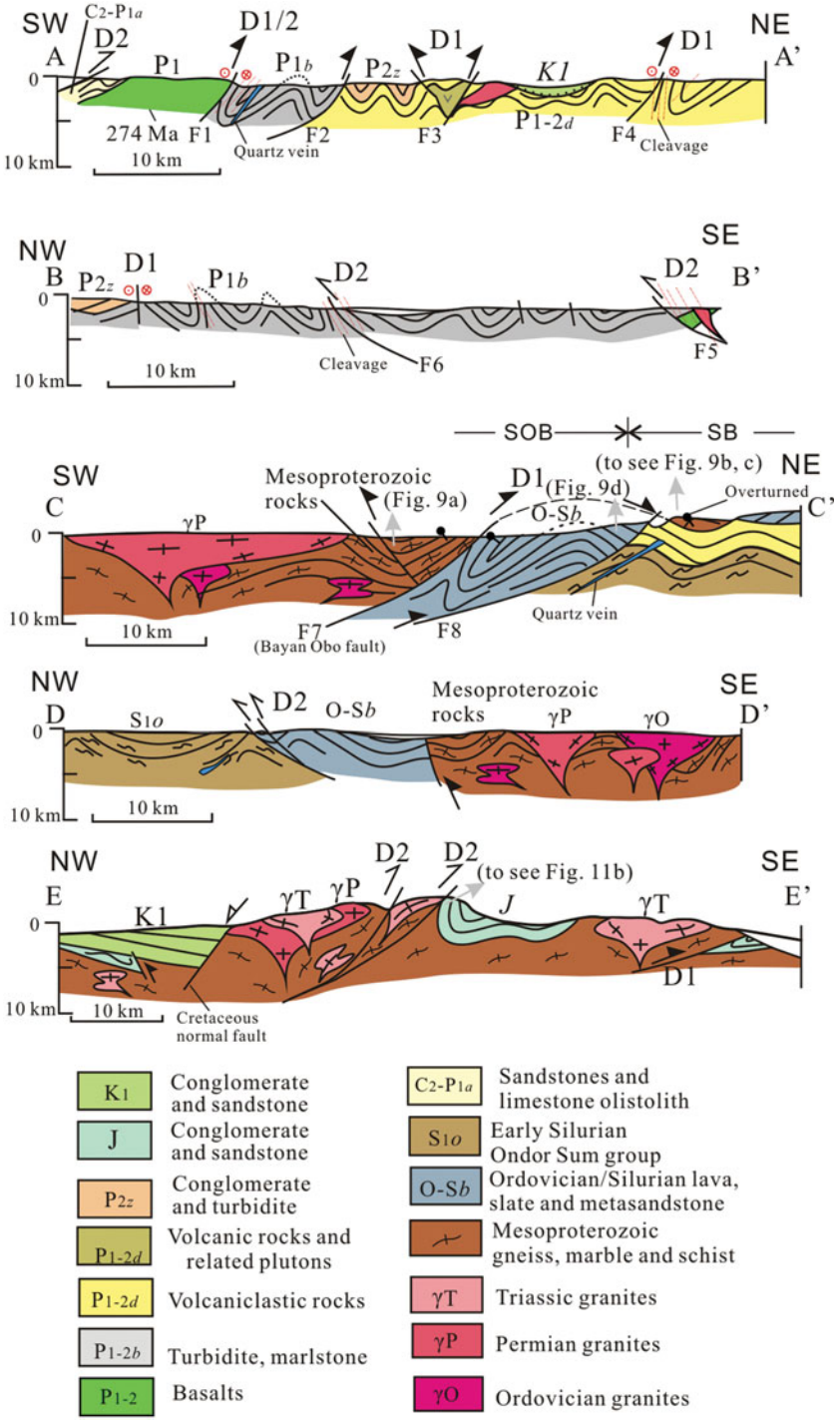

Figure 3. (Colour online) Representative cross-sections through the Solonker tectonic zone (A–A′, B–B′, C–C′), the Southern Orogenic Belt (C–C′, D–D′) and the Langshan range (E–E′), illustrating the structural style of the Mesozoic tectonics. (The section locations are in Fig. 1c, Fig. 2 and Fig. 8). D1 and D2 refer to the deformation phases described in the text. SB – Solonker Belt; SOB – Southern Orogenic Belt.

The Ordovician meta-volcanic rocks were thrust above the Ondor Sum Group and the Permian volcaniclastic rocks of the Baotege Formation by the F8 fault (Fig. 3 C–C′). The meta-volcanic rocks near the F8 fault developed WNW–ESE-trending, nearly vertical foliation, and the amygdaloidal structures with calcite infillings are sheared to form shear bands (Fig. 9d). In the microscopic view, the nearly vertical stretching lineation is defined by elongated phenocrysts, and the kinematic indicators suggest a top-to-the-NNE sense of shear (Fig. 9e).

Like the Mandula area, the Ganqi area also has a group of NE–SW-trending faults. Some of the faults display transpressional features.

The Mesoproterozoic meta-sedimentary rocks have predominant beds/foliations dipping to the NW or SE, but also have NNE or SSW dips (Fig. 8). As seen in outcrop, the Mesoproterozoic meta-sedimentary

https://doi.org/10.1017/S0016756818000183 Published online by Cambridge University Press

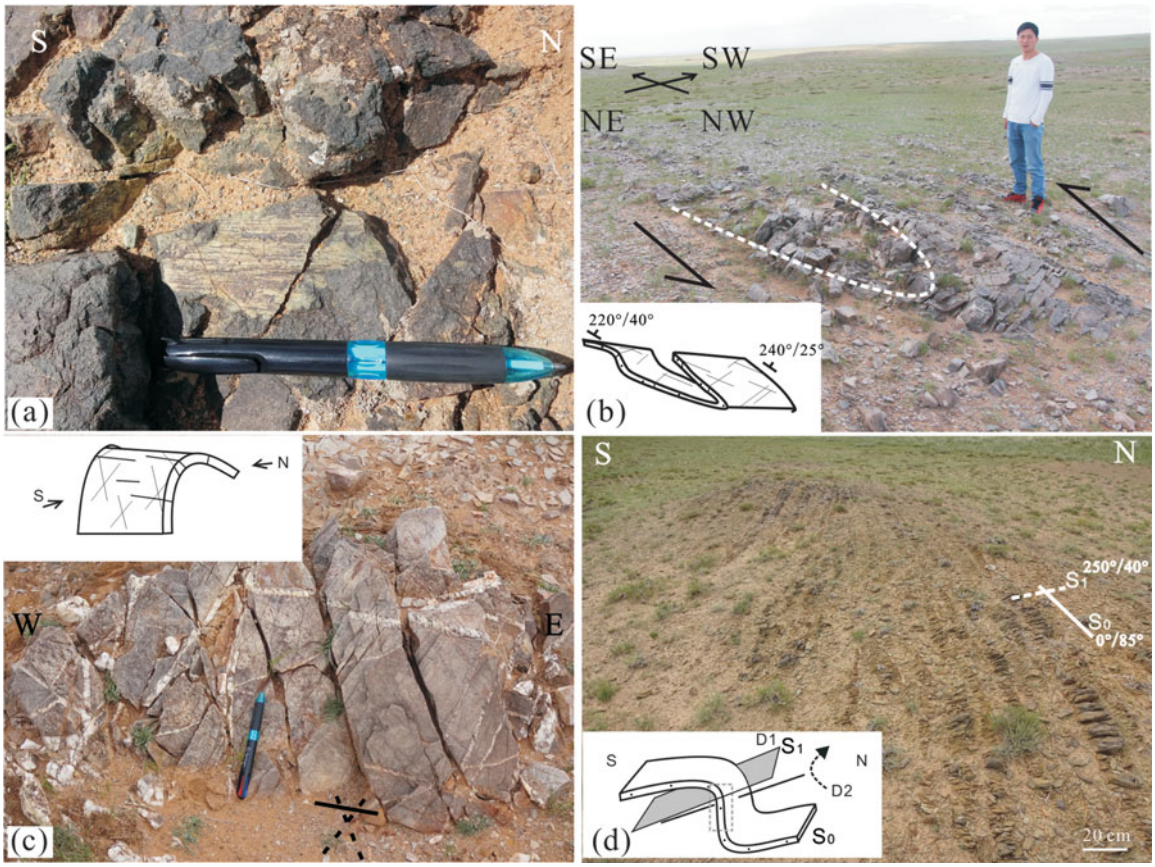

Figure 4. (Colour online) Field pictures of the D1 stage deformation in the Mandula area. (a) N–S-trending striae in the basalts (Early Permian), immediately south of the F1 fault. Length of pen for scale is 15 cm. (b) Drag fold preserved in the folded turbidite (Baotege Formation, Early Permian, GPS: 42° 23′ 22″ N, 110° 17′ 07″ E); the strata are overturned to the north, indicating a northward thrust with left lateral strike-slip components, immediately north of the F1 fault. Height of man for scale is *c*. 175 cm. (c) Two sets of shear joints and a set of tensional joints developed in the Permian turbidite (Baotege Formation, Early Permian; GPS: 42° 23′ 35″ N, 110° 16′ 33″ E). Quartz veins of Middle Triassic ages fill the joints (see Section 4 in the text). Length of pen for scale is 15 cm. (d) Intersection of the bed and cleavage indicates two stages of deformation: the D1 of NNE–SSW contraction produced N-verging asymmetric folds and related cleavages (S1); the D2 of NW–SE contraction rotated the cleavage planes, found in the Lower and Middle Permian Dashizhai Formation (GPS: 42° 39′ 28″ N, 110° 22′ 50″ E).

rocks developed crenulation in the bedding plane (here named as pre-D1). The pre-D1 crenulation was overlain by a NE–SW slicken lineation caused by interlayer sliding (Fig. 10a, b), and the beds developed a cleavage that now dips to the west. Both the cleavage and the NE–SW slicken lineation indicate the early stage (D1) of NNE-verging asymmetric folding. Subsequently, the early structures were rotated by the later stage (D2) of deformation so that the beds are now overturned to the SE and the cleavage dips to the west (Fig. 10a, b). The Ordovician meta-volcanic rocks also have some foliations dipping to the NW or SE (Fig. 3 D–D′).

The Ordovician and Silurian Ondor Sum Group is the subduction mélange corresponding to the Early Palaeozoic subduction event; it becomes difficult to distinguish the deformation related to the Early Palaeozoic subduction-related fabrics from the late-stage structures. All the foliations of the Ondor Sum Group plotted in a large range around N–S (Fig. 8). The folded sericite schist, striking E–W, developed a S-dipping cleavage that was filled by quartz veins (Fig. 10c). However, the sericite quartz schist of the Ondor Sum Group in places developed kink bands, resulting from a NW–SE contraction (Fig. 10d). The crenulation lineation of the early stage (D1 or Pre-D1) sometimes dips to the NW or SE (Fig. 11a).

3.b.3. Interpretation

In addition to the deformation of the Ordovician–Silurian rocks inherited from the Early Palaeozoic event, two main deformation stages can be identified according to the superimposed structures. The first stage of deformation (D1) developed the NNE-directed thrusts, klippe above the Permian rocks and the NNE (N)- or SSW (S)-dipping foliations, implying a nearly NNE–SSW contraction. The second stage of deformation (D2) reworked the early structures. The D2 stage of deformation resulted from a NW–SE contraction as suggested by the NW- and SE-dipping foliation and the small NW-trending transpressional faults. The NNE- or SSW-dipping foliations (D1) were refolded by the later approximately orthogonal contraction (D2) to form the fold interference patterns (Fig. 7).

https://doi.org/10.1017/S0016756818000183 Published online by Cambridge University Press

Table 1. The main thrust faults in the Mandula and Ganqi areas

Fault No.	Study area	Involved strata	Strike	Slip	Kinematics (and kinematic evidence)	Stage
F1	Mandula area	The boundary between the Permian basalts and the Lower Permian Baotege Formation	WNW–ESE	SW or SSW	NNE-directed thrust (striae in the basalts and SW-dipping overturned strata in the turbidite); sinistral strike-slip movement (locally preserved drag folds in the turbidite)	D1
F2	Mandula area	The boundary between the Lower Permian Baotege Formation and the Middle Permian Zhesi Formation	NW–SE	SW	NE-directed thrust (the turbidite of the Baotege Formation near the fault develops SW-dipping foliation and geometrically overlies the conglomerates of the Zhesi Formation)	D1
F3	Mandula area	The Lower and Middle Permian Dashizhai Formation, commonly developed along the boundary of the massive volcanic rocks and the turbidite	WNW–ESE	SSW or S	NNE-directed thrust with strike-slip component (the strata are vertical with a series of vertical, net-like joints)	D1
F4	Mandula area	The boundary between the Middle Permian Zhesi Formation and the Lower and Middle Permian Dashizhai Formation	W–E	S or SSE	NNE-directed thrust (N-verging asymmetric folds developed in the sandstones near the fault) with strike-slip component (locally preserved plunging vertical folds)	D1
F5	Mandula area	Cross-cutting the Lower and Middle Permian strata and magmatic rocks	NE–SW	SE	NW-directed thrust (kinematic indicators of the elongated quartz and feldspar in the mylonitic rocks)	D2
F6	Mandula area	Cross-cutting the Lower and Middle Permian strata	NE–SW	SE	NW-directed thrust (kinematic indicators in the mylonitic rocks)	D2
F7 (Bayan Obo fault)	Ganqi	The boundary between the Mesoproterozoic rocks and the Ordovician and Silurian meta-volcanic rocks	WNW–ESE	S or SSW	NNE-directed thrust (S-dipping foliation in the Mesoproterozoic rocks and northward overturned meta-volcanic rocks in the north of the fault)	D1
F8	Ganqi	The boundary between the Ordovician and Silurian meta-volcanic rocks and the Permian sedimentary rocks	WNW–ESE	SSW	NNE-directed thrust (S-dipping foliation near the fault, and kinematic indicators in the mylonitic Ordovician meta-volcanic rocks)	D1

Figure 5. (Colour online) Photographs of NW- or SE-directed thrusts of the D2 stage of deformation in the Mandula area. (a) Mylonitic granites preserved in the F5 thrust faults (GPS: 42° 25′ 08″ N, 110° 27′ 41″ E). (b) Microfabrics show a top-to-the-NW shearing; Qz – quartz. (c) Foliated marlstones (the Baotege Formation, Early Permian) along the F6 fault. (d) Sigmoidal porphyroclast of feldspar showing a top-to-the-NW sense of shear in the mylonitic sandstones of the F6 fault; Fld – feldspar. (e) SE-directed thrust (D2) cross-cuts the N-dipping turbidite (D1), found in the Lower to Middle Permian Dashizhai Formation; the fault plane (S_F) dips to the NW and the beds (S_0) dip to N. (f) Fault breccias and mirror surface with pseudotachylite are observed close to the fault. Length of pen for scale is 15 cm.

3.c. The Langshan range (the northern Yinshan Belt)

3.c.1. Lithostratigraphy and magmatic rocks

The NE–SW-trending Langshan range is *c.* 80 km in width. The basement rocks comprise Neoarchaean to Palaeoproterozoic gneiss, and Meso- to Neoproterozoic meta-sedimentary and meta-volcanic rocks (Hu *et al.* 2014). Upper Palaeozoic sandstone, limestone and volcanic rocks are locally exposed. The Mesoproterozoic basement rocks are unconformably overlain by Jurassic and Cretaceous sequences (Fig. 1c; NMBGMR, 1991). The Jurassic sequences,

https://doi.org/10.1017/S0016756818000183 Published online by Cambridge University Press

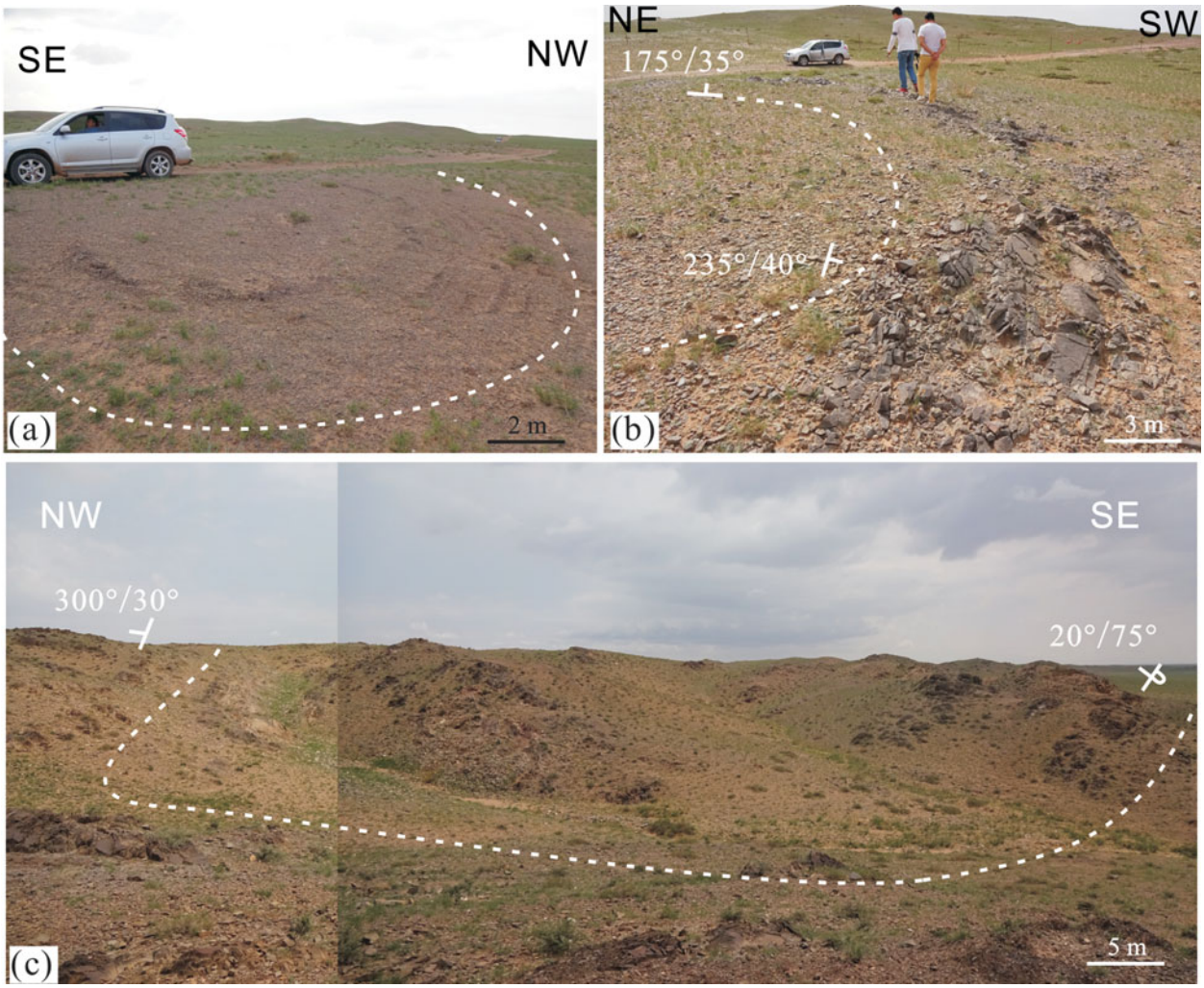

Figure 6. (Colour online) Field photos of the superimposed folds in the Mandula area. (a) Dome structure in the siltstones (Baotege Formation, Early Permian; GPS: 42° 24′ 38″ N, 110° 17′ 06″ E). (b) Dome structure in fine-grained turbidite (Dashizhai Formation, Early and Middle Permian). (c) Superimposed fold (dome) preserved in the Permian volcaniclastic rocks (Dashizhai Formation, Early and Middle Permian; GPS: 42° 39′ 30″ N, 110° 21′ 56″ E). The strata dipping to the NE is overturned. The wavelength of the fold is *c*. 100 m, which is larger than folds observed in the siltstones (a) and (b).

the Shiguai Group, of more than 1 km thickness, are composed of conglomerate, sandstone and shale (NMBGMR, 1991), and the Cretaceous strata, of more than 2.5 km thickness, are composed of conglomerate, sandstone and shale. The Langshan range consists of magmatic rocks of Early Permian (294–272 Ma), Late Permian (260–254 Ma) and Middle–Late Triassic (245–227 Ma; Wang, Z. Z. *et al.* 2015, 2016; Feng *et al.* 2017) ages. The Triassic igneous rocks are characterized by biotite-granite and biotite-, K-feldspar-granite (NMBGMR, 1991).

3.c.2. *Polyphase deformation*

Here we present a transverse section from SE to NW to show the framework of the Langshan range (Fig. 3 E–E′). The Mesoproterozoic rocks near the Ordos basin were thrust to the southeast by a high-angle thrust fault, over the Jurassic conglomerates and sandstones (Fig. 11b). The Jurassic strata were folded into a series of NE-trending open folds. Northwardly, in the central part of Langshan range, the Mesoproterozoic rocks were intruded by large amounts of Permian and Triassic gneissic granites (Fig. 3 E–E′). The foliation of the gneissic granite mostly dips to the north. Further to the northwest, the Mesoproterozoic meta-sedimentary rocks are characterized by NW-directed imbricated sheets (Fig. 11c).

The main tectonic line changes to NNE-trending on the western side of the Langshan range. Large volumes of Permian granites and minor gneissic biotite-granite plutons distribute along the western side of the Langshan range. The Permian plutons developed two sets of joints, along which the crystals recrystallized to become coarser (Fig. 11d). The gneissic biotite-granite plutons with predominant ESE-dipping foliations bear WNW-directed stretching lineations defined by oriented biotite and muscovite (Fig. 11e, f).

All the deformed rocks are unconformably covered by the Cretaceous sedimentary rocks (Fig. 3 E–E′).

https://doi.org/10.1017/S0016756818000183 Published online by Cambridge University Press

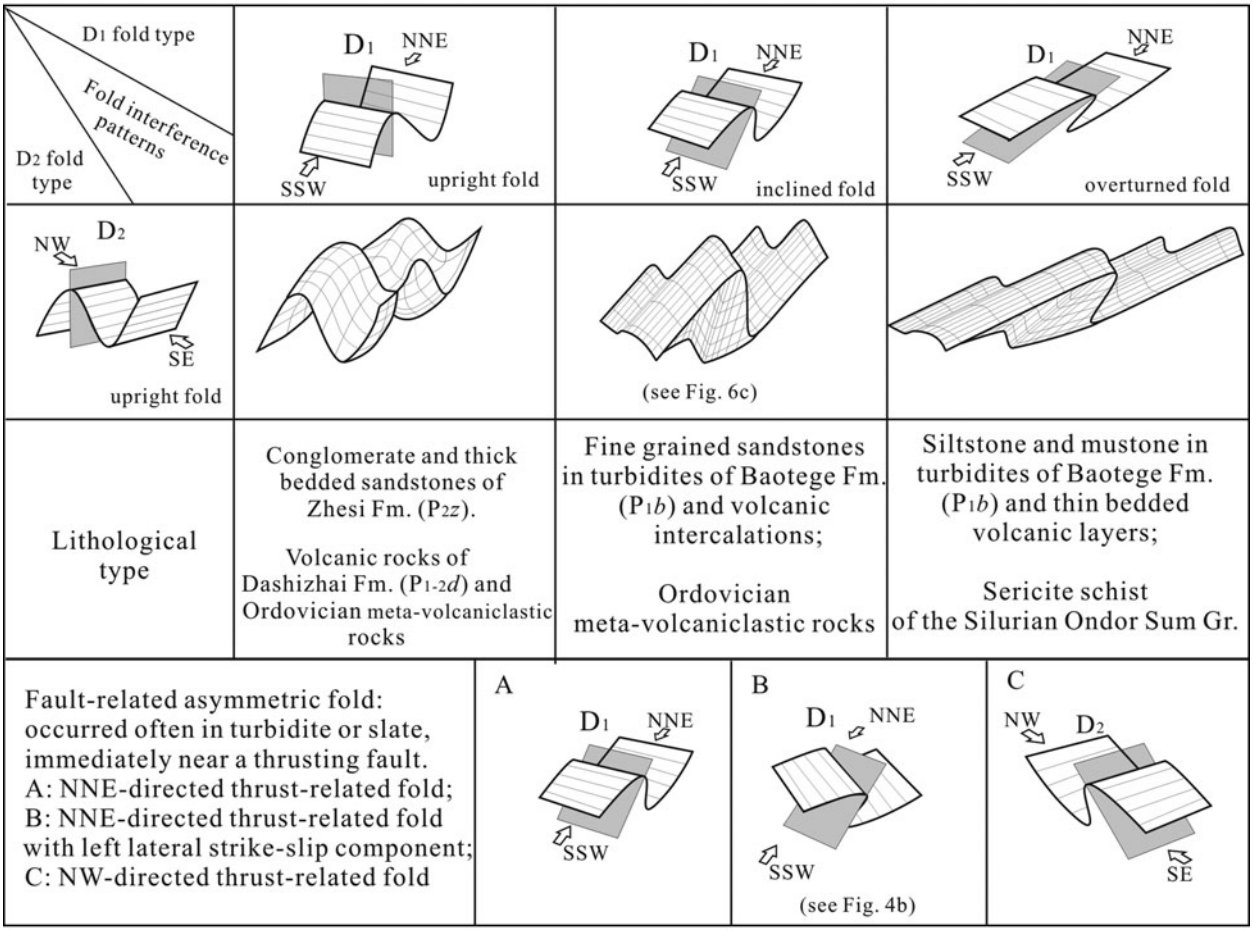

Figure 7. Block diagrams showing the fold interference patterns created by the two stages of deformation in the Mandula and Ganqi areas.

3.c.3. Interpretation

The deformation in the Langshan range is related to two stages of deformation. The first stage (D1) developed the nearly E–W-striking foliation in the Permian granitic rocks and the locally ductile deformation of the Triassic gneissic granites, indicating a nearly NNE–SSW contraction. The second stage (D2) developed the SE-directed thrust fault and NE-trending folds in the Jurassic strata and the NW-directed imbricated sheets in the Mesoproterozoic rocks, indicating a NW–SE contraction. The conjugate joints in the granitic plutons and the lineation in the gneissic biotite-granite suggest the contraction was WNW–ESE on the western side of the Langshan range, which is probably related to strain partitioning of the NW–SE contraction along the NNE–SSW-trending boundary faults, the Langshan fault (Zhang, J. *et al.* 2014) or the Zuunbayan fault (Webb, Johnson & Minjin, 2010). The NNE–SSW-trending boundary fault might previously have been a strike-slip fault caused by the NNE–SSW contraction of the D1 stage.

To summarize, the study region (including the Solonker Belt, the Southern Orogenic Belt and the northern Yinshan Belt) underwent two stages of deformation during the Mesozoic period. In the Mandula area of the Solonker Belt, the D1 stage of deformation led to the development of the NNE-directed thrusts and a series of WNW–ESE-trending, NNE-verging folds (Table 1; Fig. 7). The D2 stage of deformation formed the NW-directed thrusts and NE–SW-trending folds. The sedimentary rocks were folded by the two nearly orthogonal contractions to form basin-and-dome or mega arrowhead-shaped fold patterns (Fig. 7; e.g. Ramsay & Huber, 1987; Deng, Koyi & Nilfouroushan, 2016). In the Ganqi area, the Mesoproterozoic rocks and the Early Palaeozoic meta-volcanic rocks are exposed as tectonic nappes thrust to the NNE over the Permian volcaniclastic rocks during the D1 stage. The rock foliation was refolded by the D2 stage of NW–SE contraction. In the Langshan range, the N- or NNE-dipping foliation of the Triassic gneissic granites suggests the D1 stage of deformation. The D2 stage of NW–SE contraction is responsible for the development of SE- or NW-directed thrusts in the Mesoproterozoic rocks and NE-trending folds in the Jurassic sedimentary rocks.

4. Dating of the quartz veins

We chose quartz vein samples for zircon dating to constrain the deformation age. The quartz veins are ore veins of hydrothermal origins with a significant

https://doi.org/10.1017/S0016756818000183 Published online by Cambridge University Press

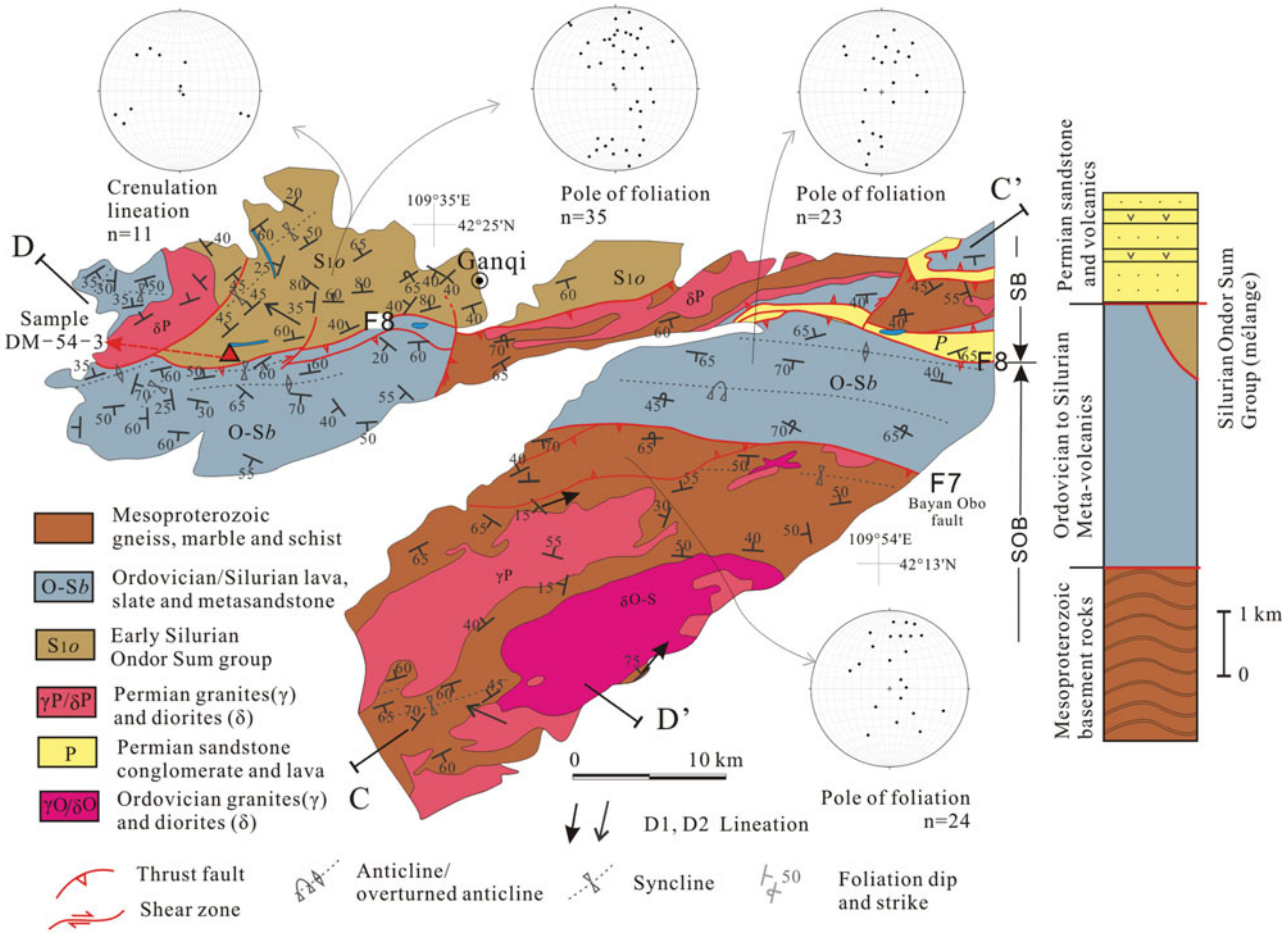

Figure 8. (Colour online) Geological and structural map of the Ganqi area and lower hemisphere projections of the measured structural data.

amount of Au. In the field, the quartz veins cut the Permian strata along the joints (Fig. 4c), or intrude along the cleavages of asymmetric folds (Fig. 10c). Zircon grains were separated using conventional heavy liquid and magnetic techniques. The grains were then hand-picked and mounted within epoxy resin discs, and then polished to expose their internal structures. The internal morphology of the zircons was examined using cathodoluminescence (CL) prior to U–Pb isotopic analyses. The CL imaging and U–Pb dating by laser ablation inductively coupled plasma mass spectrometry (LA-ICP-MS) were conducted at the Sample Solution Analytical Technology Co. Ltd Wuhan with analysed spot sizes of 32 μm. Detailed operating conditions for the laser and ICP-MS instrument followed Liu *et al.* (2008) and Lin *et al.* (2015). The measured data are listed in the online Supplementary Material available at http://journals.cambridge.org/geo.

Hydrothermal zircon may directly precipitate or form through the alteration of magmatic zircon by aqueous fluids exsolved from highly evolved magmas (Schaltegger, 2007). Igneous zircon in hydrothermal environments is easily altered by aqueous fluid, causing secondary textures that cut across the primary growth zone (Corfu *et al.* 2003; Hoskin, 2005; Geisler, Schaltegger & Tomaschek, 2007). The secondary textures overprinting the primary zircon domains often present as patchy areas, sector zoning, a porous texture or as homogeneous without zoning (Hoskin, 2005; McNaughton, Mueller & Groves, 2005; Lawrie *et al.* 2007; Pelleter *et al.* 2007; Park *et al.* 2016). In addition, typical hydrothermal zircons contain fluid inclusions (e.g. Zhu *et al.* 2017; Fig. 12).

Sample DM-14-3 was taken in the Mandula area (Fig. 2). The quartz vein intruded the Permian turbidites which were folded by the D1 deformation (Fig. 4c). Zircon grains separated from sample DM-14-3 are yellow to light brown, translucent and have a sub-rounded, elongated grain morphology, ranging in length from 50 to 100 μm. Some zircon grains have inhomogeneous internal textures (Fig. 12). The well-developed magmatic oscillatory zoning is overlain by patchy sectors, corresponding to the reworking of hydrothermal fluids (Fig. 13a). Twenty-five spots were analysed and the youngest five grains yield a mean age of 226 ± 3 Ma (MSWD = 0.98; Fig. 13a, b). The other grains with relatively older ages are considered as inherited zircons.

Sample DM-45-1 was also taken in the Mandula area (Fig. 2). The quartz vein intruded the Permian turbidites along joints. Zircon grains separated from sample DM-45-1 range from 50 to

https://doi.org/10.1017/S0016756818000183 Published online by Cambridge University Press

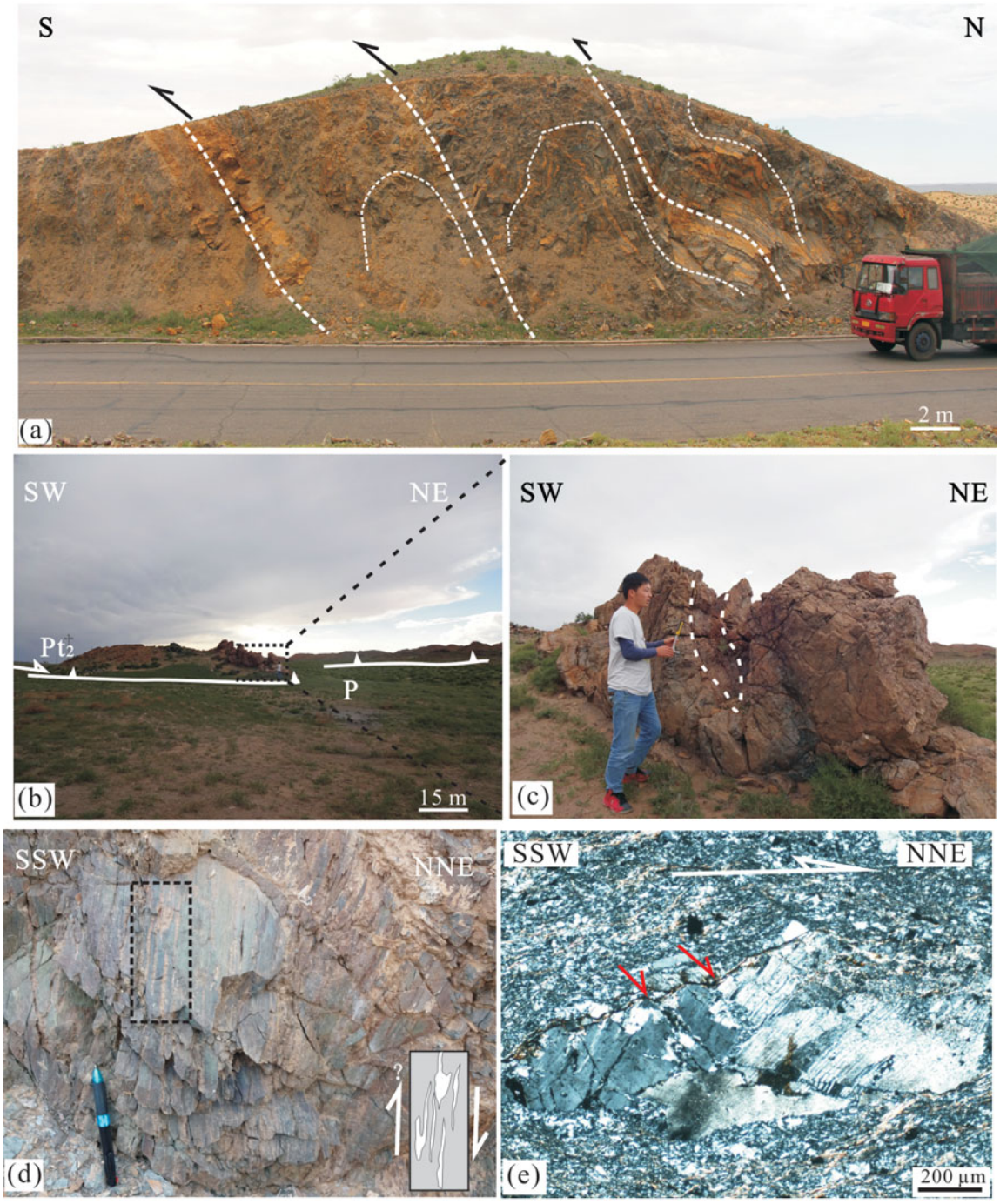

Figure 9. (Colour online) Field photos of structures related to the NNE-directed thrust in the Ganqi area. (a) The banded amphibolites include imbricated S-verging asymmetric fold sheets (GPS: 42° 16′ 56″ N, 107° 38′ 49″ E). The thrusts among the sheets are antithetic faults of the main thrust F7 (Bayan Obo fault). (b) Macroscopic view of the klippe (GPS: 42° 21′ 40″ N, 107° 38′ 08″ E). The klippe is composed of Mesoproterozoic marbles and clastic rocks. The underlying rocks are the Permian folded volcaniclastic rocks and turbidites. (c) Enlarged view of one klippe showing the marble developed intraformational folds. Height of man for scale is *c*. 175 cm. (d) The intensively sheared Ordovician meta-volcanic rocks near the F8 fault. The white shear bands are stretched calcites filling in the amygdaloidal structures. Length of pen for scale is 15 cm. (e) Oblique fractured porphyroblast suggests a top-to-the-NNE shearing, from the Ordovician meta-volcanic rocks of (d).

150 μm in length. A total of 30 spots were analysed and the five youngest grains cluster at the age of 236 ± 6 Ma (MSWD = 0.13; Fig. 13). The grains with Triassic ages show weak oscillatory zoning overlain by irregular sectors because of hydrothermal fluid reworking. The grains with ages in the range *c*. 310 Ma, 410–450 Ma and Precambrian ages are interpreted as inherited zircons.

Sample DM-54-3 was taken in the Ganqi area (Fig. 8). The quartz vein intruded the Lower Palaeozoic Ondor Sum Group along the cleavages of a D1 fold (Fig. 10c). The zircon grains are elongated to

https://doi.org/10.1017/S0016756818000183 Published online by Cambridge University Press

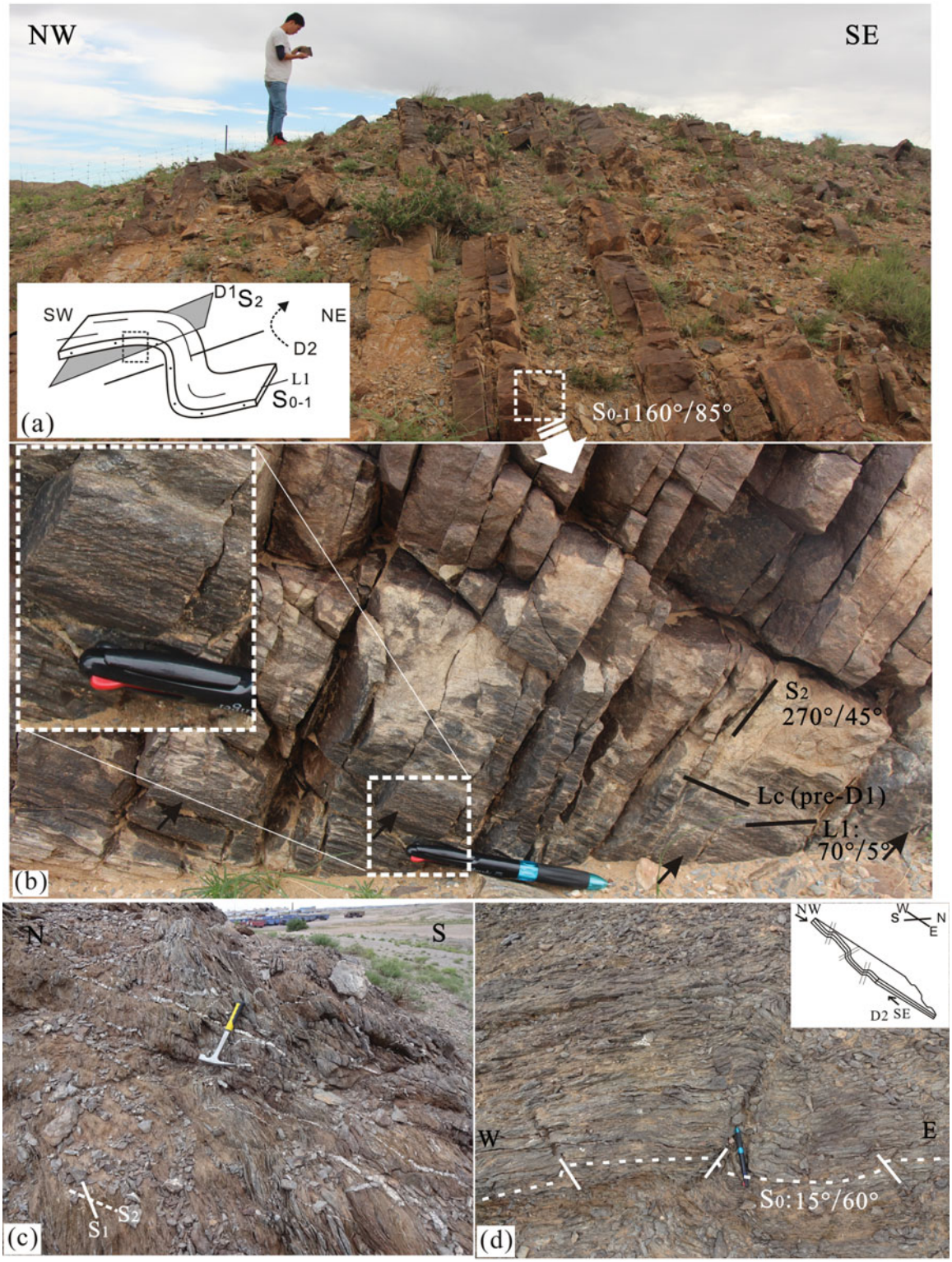

Figure 10. (Colour online) Superimposed folds in the Ganqi area. (a) The meta-sedimentary rocks bear multiple stages of structures (GPS: 42° 17′ 10″ N, 107° 38′ 35″ E). The current strata ($S_{0\text{-}1}$) are overturned, dipping to the SE. (b) On the basal surface, the crenulation lineation (Lc) represents the pre-D1 fabric, which is overprinted by striae lineation (L_1, marked by black arrows and see enlarged inset) caused by interlayer sliding of the D1 folding. The cleavage (S_2) is produced by the D1 NE- or NNE-verging folds but was rotated by the D2 stage of NW–SE contraction (see text for more detailed explanations). (c) The sericite schist rocks (S_1, reference surface) in the Ondor Sum Group are refolded and produce the S2 cleavages which are filled by quartz veins. (d) The N-dipping (D1) sericite quartz schist was overprinted by a kink band structure (D2), found in the Ondor Sum Group. Length of pen is 15 cm, length of hammer is 25 cm and height of man is *c*. 175 cm for scale.

https://doi.org/10.1017/S0016756818000183 Published online by Cambridge University Press

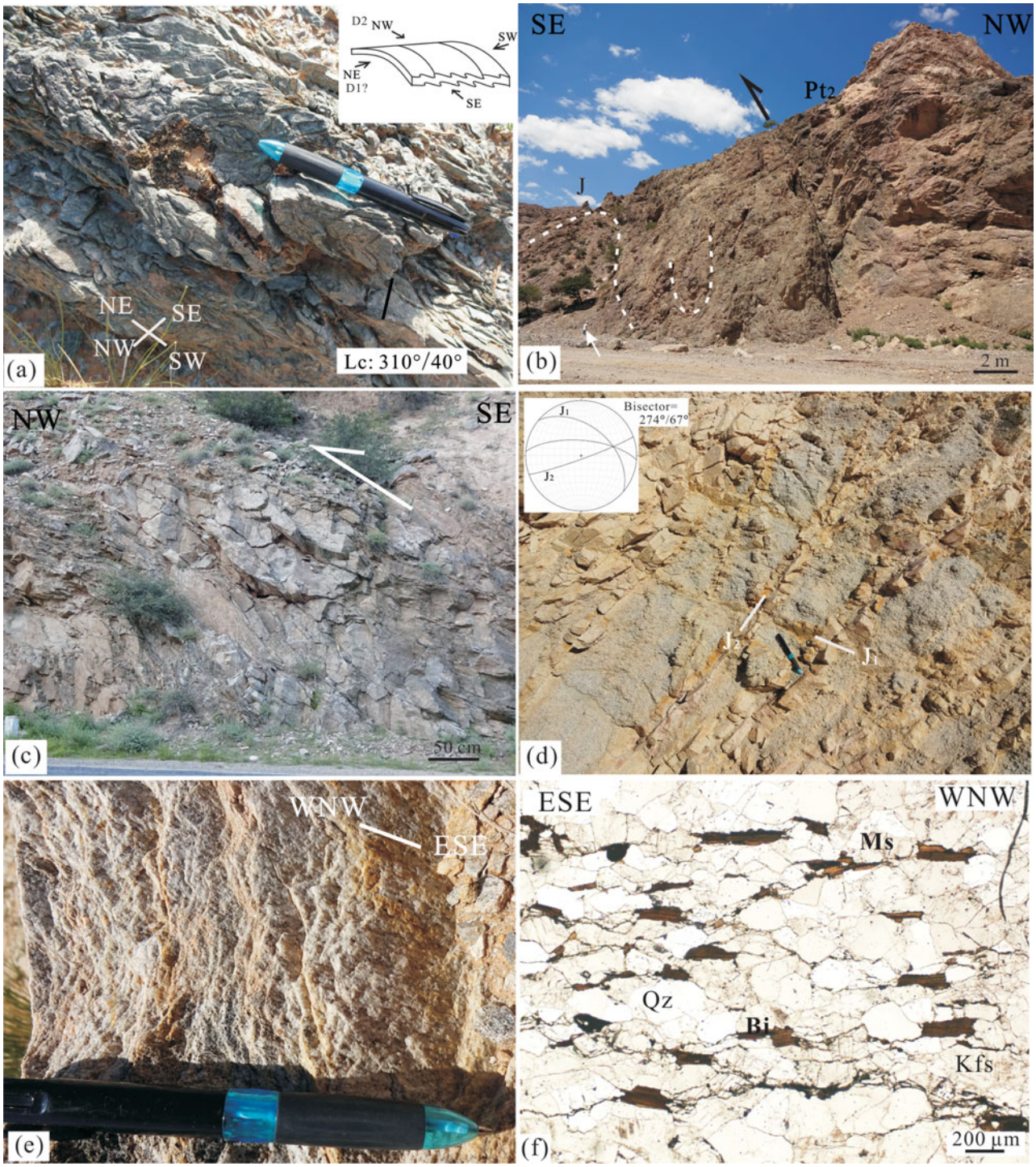

Figure 11. (Colour online) Field photos in the Ganqi area and the Langshan range. (a) The crenulation lineation is inclined by the D2 stage of NW–SE contraction, found in the sericite quartz schist of the Ondor Sum Group, Ganqi area. (b) The Mesoproterozoic gneissic complexes thrust onto the Jurassic conglomerates through a high-angle fault; the high-angle thrust is probably reversed from a normal fault linked with Early Jurassic extension, found on the southeastern side of the Langshan range (GPS: 41° 18′ 33″ N, 107° 29′ 28″ E). (c) Outcrop-scale sigmoidal structures in the Mesoproterozoic meta-sedimentary rocks imply a series of NW-verging imbricated sheets. (d) Conjugate joints in the Permian plutons are filled with coarser-grained granitic veins. The bisector of the two sets of joints indicates a nearly E–W contraction. (e) The gneissic biotite granites on the western side of the Langshan range (foliation dip: 110°/25°). (f) The WNW–ESE stretching lineation is defined by the oriented biotite and quartz; Bi – biotite; Ms – muscovite; Qz – quartz; Kfs – K-feldspar. Length of pen is 15 cm and height of man is *c*. 175 cm for scale.

ellipsoidal in shape with grain sizes of 50–100 μm (Fig. 12). Most of the grains show misted structures without clear zoning. A total of 20 spots were analysed and five grains cluster at 226 ± 5 Ma (MSWD = 0.45; Fig. 13). The grains with Palaeozoic and Precambrian ages are considered to be inherited zircons. Several grains plot away from the concordia curve, which is probably caused by Pb loss.

Sample DM-77-2 was taken on the western side of the Langshan range (Fig. 1c). In the outcrops, the

https://doi.org/10.1017/S0016756818000183 Published online by Cambridge University Press

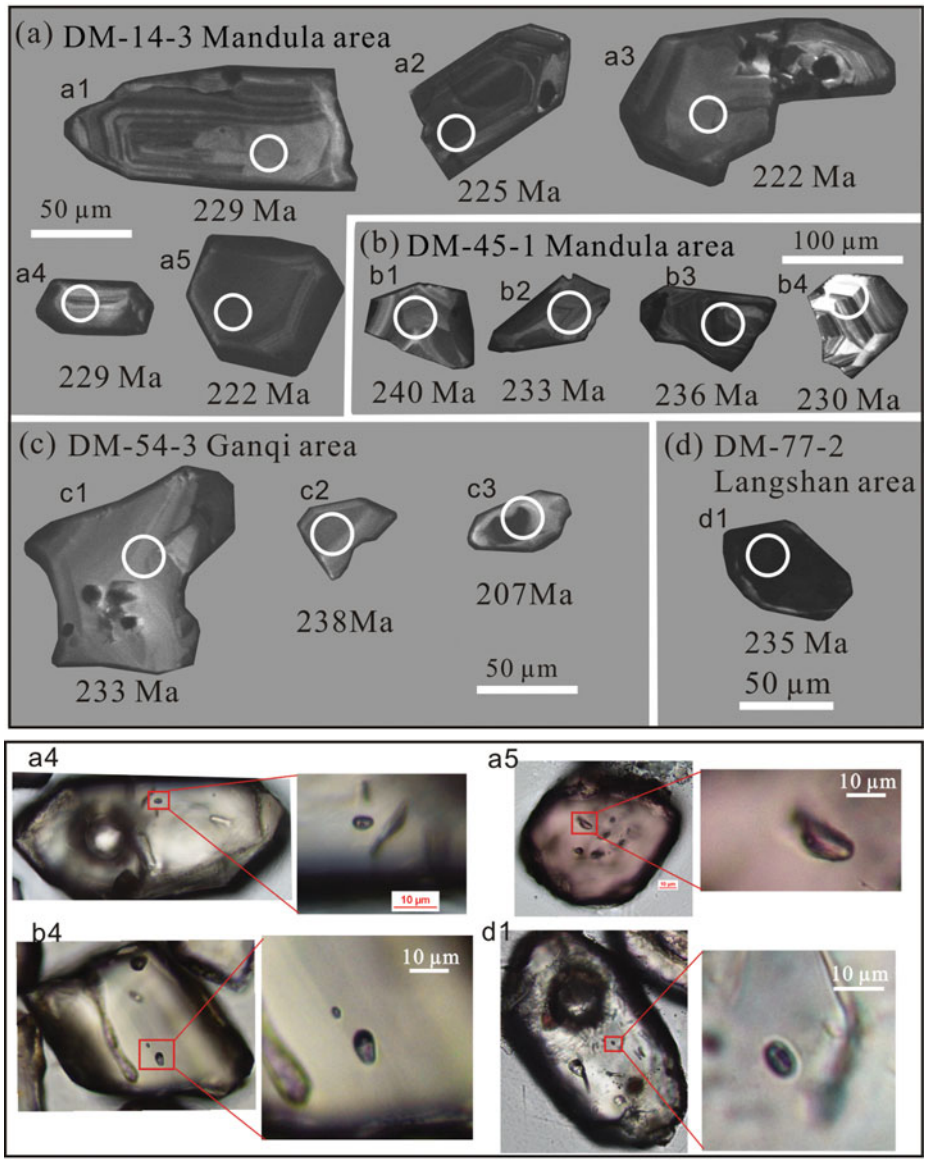

Figure 12. (Colour online) Representative CL images and fluid inclusions of the analysed zircons. Ages (Ma) and analysed spots (circles) are marked on the zircons. Patchy texture overprints oscillatory zoning of primary zircons as shown in a1, a2, a3, b2, b4; zircons that are homogeneous without clear zoning are shown in a4, c2, c3; zircons with irregular morphology are b3, c1; zircons with contrasting mantle texture are a4, a5, c3, d1.

Mesoproterozoic meta-sandstones trend WNW–ESE due to the D1 deformation and are cross-cut by the quartz vein. Zircon grains from sample DM-77-2 are ellipsoidal in shape with grain sizes of 50–100 μm. Some grains show homogeneous textures or dark inner cores (Fig. 12). Only one zircon grain yields a concordant Triassic age of 236 ± 2 Ma. Several grains do not plot on the concordia curve, which is probably caused by Pb loss. Three zircon grains yield a lower intercept age of 235 ± 4 Ma (MSWD = 1.4; Fig. 13).

5. Discussion

5.a. The timing of the D1 and D2 stages of deformation

The two shear joints apparently comprise conjugate joint sets with a nearly NNE–SSW direction of the acute angle bisector (Fig. 4c), which is consistent with the NNE–SSW contraction of the D1 deformation. The quartz veins filled the joints or the cleavages of the folded strata/foliations (Figs 4c, 10c). Thus, we consider that the formation age of the quartz veins is identical to or younger than the age of the D1 deformation. Some zircons obtained from the quartz veins show internal textures of patchy sectors or misted structures without clear zoning, which are features of zircons reworked by hydrothermal fluids. Therefore, the hydrothermal zircons represent the formation age of the quartz veins. These zircons generally yield Middle Triassic ages.

It should be noted that the dated zircon ages are not absolutely valid, because we cannot exclude the hydrothermal zircons from also being inherited ones, like the other zircons of older ages. The joints are of brittle deformation, which cannot be excluded from being the

https://doi.org/10.1017/S0016756818000183 Published online by Cambridge University Press

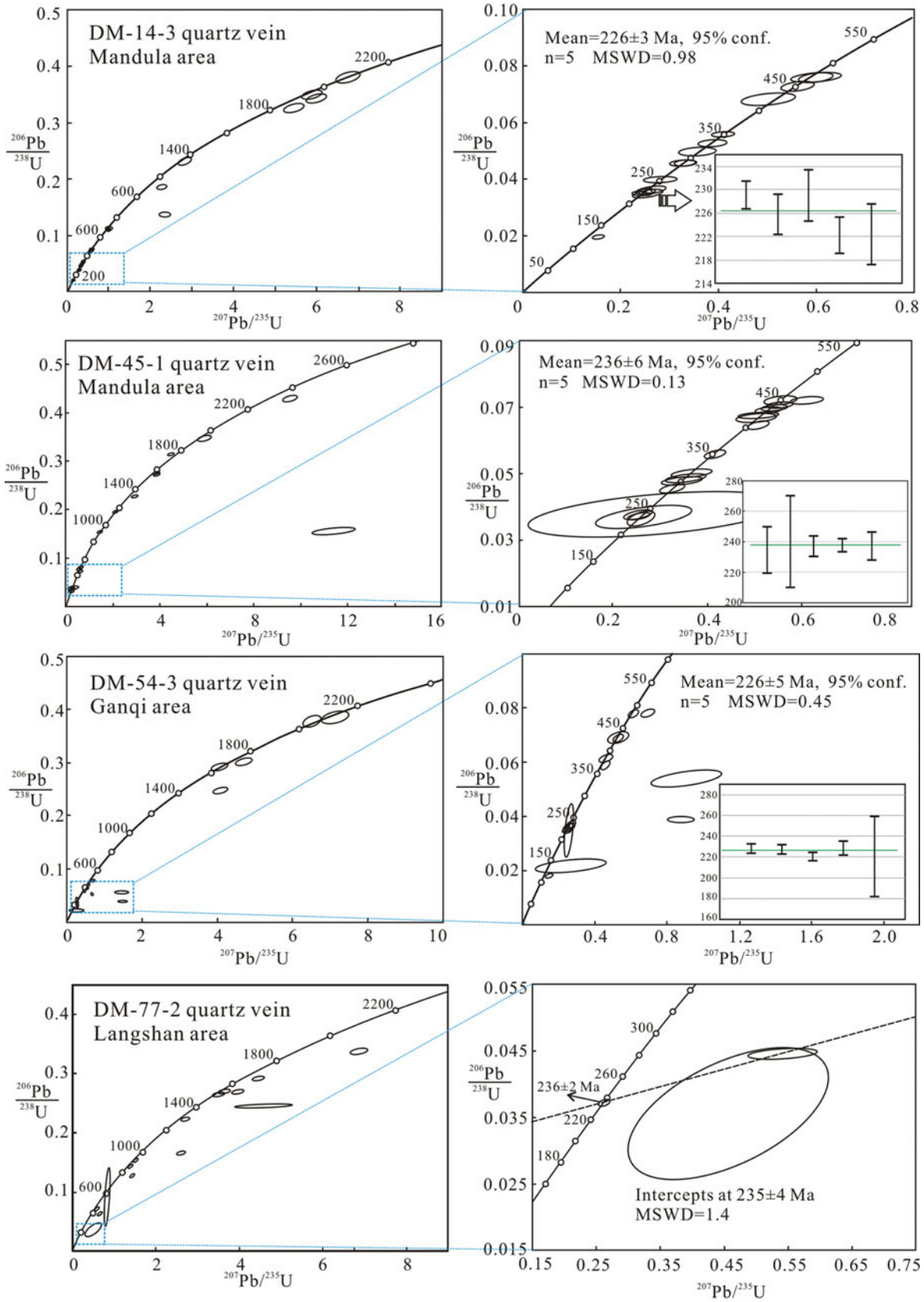

Figure 13. (Colour online) Zircon U–Pb concordia diagrams for the analysed quartz vein samples. Samples DM-14-3 and DM-54-3 have three discordant Cretaceous age grains probably caused by Pb loss, and sample DM-77-2 has only one grain of age 236 ± 2 Ma (see age data in online Supplementary Material available at http://journals.cambridge.org/geo).

https://doi.org/10.1017/S0016756818000183 Published online by Cambridge University Press

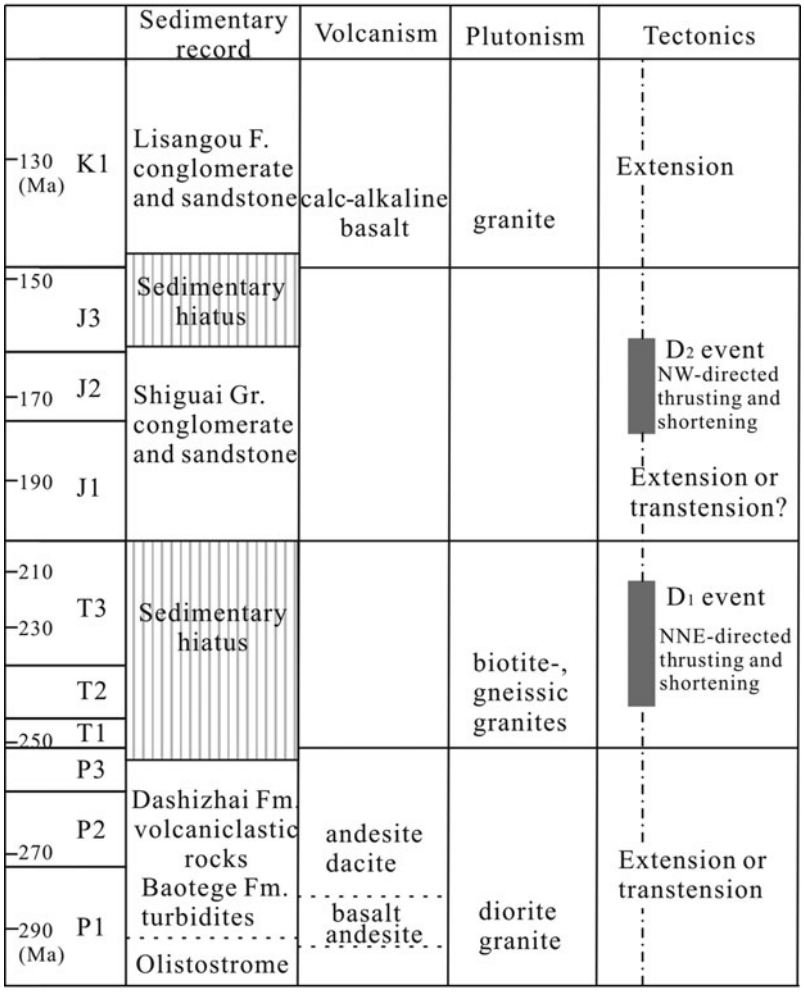

Figure 14. Synoptic table of the Late Permian to Early Cretaceous volcanic, plutonic and sedimentary rocks and tectonic events in the Mandula and Ganqi areas showing the timing of the two tectonic events.

result of a much later stage of deformation. However, we note that there is a significant sedimentary hiatus during the Triassic Period (NMBGMR, 1991; Fig. 14). Furthermore, geothermal modelling by detrital apatite fission tracks in the Mandula area suggested that there were high rates of cooling (1.3 °C/Myr) during Middle to Late Triassic times, which produced a *c*. 4 km tectonic exhumation (Li *et al.* 2016). The nearly N–S shortening events were also documented in the Yinshan Belt during 237–213 Ma (muscovite Ar–Ar ages, Gao, 2010; Zhang, J. *et al.* 2014) and the Yanshan Belt during 270–190 Ma (Wang, Zhou & Li, 2011; Wang, Zhou & Zhao, 2013). Our field observations show the Jurassic rocks did not undergo the D1 stage of NNE–SSW contraction. Thus, we tend to consider, based on the above compiled data, that the D1 stage of deformation happened in Middle Triassic time.

The D2 stage of deformation may have happened during Late Jurassic time, because the Lower and Middle Jurassic sedimentary rocks of the Shiguai Group were folded by the D2 deformation and they were unconformably covered by the unfolded Lower Cretaceous strata of the Lisangou Formation (NMBGMR, 1991; Fig. 14). In addition, the Jurassic sediments, containing pebbles derived from crystalline basement, occur along a high-angle thrust fault at the mountain front (Fig. 11b). The high-angle thrust fault might be an inverted originally normal fault which was linked with a significant regional extension between the two stages (D1 and D2) of contraction (e.g. Meng *et al.* 2014; Fig. 14).

5.b. Geodynamic implications

Some studies suggest that the final closure of the Palaeo-Asian Ocean occurred during Late Permian to Middle Triassic times (e.g. Eizenhöfer *et al.* 2014; Han *et al.* 2015; Liu *et al.* 2016; Li *et al.* 2017*a*,*b*,*c*). Our studies reveal that the D1 stage of NNE–SSW contraction is characterized by N- or NNE-directed thrusting and the inferred age of the NNE–SSW contraction is about Middle Triassic, which is consistent with the tectonic models for the closure of the Palaeo-Asian Ocean (Xiao *et al.* 2003; Eizenhöfer *et al.* 2014; Han *et al.* 2015; Li *et al.* 2017*a*,*b*,*c*). Despite there being some other studies that argued that the closure of the Palaeo-Asian Ocean took place during Devonian time and the Solonker Belt switched into a rifting stage,

https://doi.org/10.1017/S0016756818000183 Published online by Cambridge University Press

producing limited ocean basins during Permian time (Xu *et al.* 2013; Chen *et al.* 2012; Shao, Tang & He, 2014; Luo *et al.* 2016), the discovery of Lower Mesozoic blueschists in East Inner Mongolia confirmed the existence of a convergent event between the limited ocean basins (Chu *et al.* 2013; Zhang, Wei & Chu, 2015; Zhang *et al*. 2016). The blueschists resulting from the closure of the embryonic, limited ocean basins are not typically of the high-pressure nature of deep subduction (Zhang, Wei & Chu, 2015; Zhang *et al*. 2016). In the case of the closure of the limited, narrow oceans, no self-sustaining subduction would likely develop owing to insufficient slab pull (Hall *et al.* 2003; Gurnis, Hall & Lavier, 2004; Chenin *et al.* 2017), and hence other Triassic geodynamic events, like the Dabie–Qinling orogeny (e.g. Dong *et al.* 2011; Huang *et al.* 2015; Li *et al.* 2016) are necessary to be employed to interpret the large scale of the nearly N–S contraction between the northern Yinshan Belt, the Southern Orogenic Belt and the Solonker Belt.

Our studies suggest that the Late Jurassic deformation (D2) is characterized by a NW–SE contraction. Some other regions adjacent to our study area also documented the Late Jurassic contraction. For example, in the Yanshan Belt, to the east of the study area, the contraction during Middle–Late Jurassic time turned to be NW–SE directed (Davis *et al.* 2001, 2002, 2009; Wang, Zhou & Li, 2011); the Helanshan area, to the south of the study area, formed NNE-trending folds during Late Jurassic to Early Cretaceous times (e.g. Darby & Ritts, 2002; Huang *et al.* 2015). The Late Jurassic NW–SE contraction was considered to be the far-field consequence of the convergence in the Mongol-Okhotsk Ocean in Far East Asia (Davis *et al.* 2001) and the westward subduction of the Palaeo-Pacific Ocean (e.g. Zhu *et al.* 2005, 2009; Faure, Lin & Chen, 2012; Huang *et al.* 2015). The horizontal compressional stress was transmitted from the subduction zones and tended to concentrate in an intracontinental 'weak' zone (i.e. the pre-existing fault zones, thermally weakened zones or mechanical contrasts between lithologies). The strains were concentrated in the Solonker Belt and the Yinshan–Yanshan Belt to develop the superimposed structures of the D1 and D2 stages of deformation (e.g. Deng & Koyi, 2015).

6. Conclusion

The Solonker Belt, the Southern Orogenic Belt and the northern Yinshan Belt underwent two stages of deformation during the Mesozoic period. The D1 stage of NNE–SSW contraction is responsible for the development of the WNW-trending folds and NNE-directed thrusts. The D2 stage of NW–SE contraction gives rise to the NE-trending folds and NW- or SE-directed thrusts. The primary strata/foliations are deformed by the two nearly orthogonal or oblique contractions to form the superimposed structures. Our new U–Pb zircon ages, along with other geological constraints, suggest the D1 stage occurred in Middle Triassic time and the D2 stage occurred in Late Jurassic time. The coeval geodynamic events of the study area led us to consider that the D1 deformation is related to the final closure of the Palaeo-Asian Ocean or limited, narrow ocean basins, and the D2 deformation is related to the subduction of the Palaeo-Pacific Ocean and the closure of the Mongol-Okhotsk Ocean.

Acknowledgements. J. Charvet and other anonymous reviewers are thanked for their beneficial comments to the earlier version of this paper. This study was supported by the National Natural Science Foundation of China (No. 41402192, No. 41472084), Major National Science and Technology Programs in the "Thirteenth Five-Year" Plan period (No. 2016ZX05024-006-002), and the China Postdoctoral Science Foundation (No. 2014M562080).

Supplementary material

To view supplementary material for this article, please visit https://doi.org/10.1017/S0016756818000183

References

Badarch, G., Cunningham, W. D. & Windley, B. F. 2002. A new terrane subdivision for Mongolia: implications for the Phanerozoic crustal growth of central Asia. *Journal of Asian Earth Sciences* **21**, 87–110.

Charvet, J., Shu, L. S., Laurent-Charvet, S., Wang, B., Faure, M., Cluzel, D., Chen, Y. & De Jong, K. 2011. Palaeozoic tectonic evolution of the Tianshan belt, NW China. *Science China: Earth Sciences* **54**, 166–84.

Chen, B., Jahn, B. M., Wilde, S. & Xu, B. 2000. Two contrasting Paleozoic magmatic belts in northern Inner Mongolia, China: petrogenesis and tectonic implications. *Tectonophysics* **328**, 157–82.

Chen, C., Zhang, Z. C., Guo, Z. J., Li, J. F., Feng, Z. S. & Tang, W. H. 2012. Geochronology, geochemistry, and its geological significance of the Permian Mandula mafic rocks in Damaoqi, Inner Mongolia. *Science China: Earth Sciences* **55**, 39–52.

Chenin, P., Manatschal, G., Picazo, S., Müntener, O., Karner, G., Johnson, C. & Ulrich, M. 2017. Influence of the architecture of magma-poor hyperextended rifted margins on orogens produced by the closure of narrow versus wide oceans. *Geosphere* **13**, 1–18.

Chu, H., Zhang, J. R., Wei, C. J., Wang, H. & Ren, Y. 2013. A new interpretation of the tectonic setting and age of meta-basic volcanics in the Ondor Sum Group, Inner Mongolia. *Chinese Science Bulletin* **58**, 3580–7.

Corfu, F., Hanchar, J. M., Hoskin, P. W. & Kinny, P. 2003. Atlas of zircon textures. *Reviews in Mineralogy and Geochemistry* **53**, 469–500.

Cui, S. & Wu, Z. 1997. On the Mesozoic and Cenozoic intracontinental orogenesis of the Yanshan Area, China. In *Proceedings of the 30th International Geological Congress* (eds Y. Zheng, G. A. Davis & A. Yin), pp. 277–92. Utrecht: VSP.

Darby, B. J. & Ritts, B. D. 2002. Mesozoic contractional deformation in the middle of the Asian tectonic collage: the intraplate Western Ordos fold-thrust belt, China. *Earth and Planetary Science Letters* **205**, 13–24.

Davis, G. A., Darby, B. J., Zheng, Y. & Spell, T. L. 2002. Geometric and temporal evolution of an extensional detachment fault, Hohhot metamorphic core complex, Inner Mongolia, China. *Geology* **30**, 1003–6.

Davis, G. A., Meng, J. F., Cao, W. R. & Du, X. Q. 2009. Triassic and Jurassic tectonics in the eastern Yanshan Belt, North China: insights from the controversial Dengzhangzi Formation and its neighboring units. *Earth Science Frontiers* **16**, 69–86.

Davis, G. A., Zheng, Y., Wang, C., Darby, B. J., Zhang, Ch. & Gehrels, G. E. 2001. Mesozoic tectonic evolution of the Yanshan fold and thrust belt, with emphasis on Hebei and Liaoning provinces, northern China. In *Paleozoic and Mesozoic Tectonic Evolution of Central and Asia: From Continental Assembly to Intracontinental Deformation* (eds M. S. Hendrix & G. A. Davis), pp. 171–94. Geological Society of American Memoir 194.

De Jong, K., Xiao, W. J., Windley, B. F., Masago, H. & Lo, C. H. 2006. Ordovician $^{40}Ar/^{39}Ar$ phengite ages from the blueschist-facies Ondor Sum subduction-accretion complex (Inner Mongolia) and implications for the early Paleozoic history of continental blocks in China and adjacent areas. *American Journal of Science* **306**, 799–845.

Deng, H. L. & Koyi, H. A. 2015. Mega arrowhead interference patterns in the central part of the Yanshan Orogenic Belt, North China. *Journal of Structural Geology* **80**, 25–37.

Deng, H. L., Koyi, H. A. & Nilfouroushan, F. 2016. Superimposed folding and thrusting by two phases of mutually orthogonal or oblique shortening in analogue models. *Journal of Structural Geology* **83**, 28–45.

Dong, Y. P., Zhang, G. W., Neubauer, F., Liu, X. M., Genser, J. & Hauzenberger, C. 2011. Tectonic evolution of the Qinling orogen, China: review and synthesis. *Journal of Asian Earth Sciences* **41**, 213–37.

Eizenhöfer, P. R., Zhao, G. C., Sun, M., Zhang, J., Han, Y. G. & Hou, W. Z. 2015a. Geochronological and Hf isotopic variability of detrital zircons in Paleozoic strata across the accretionary collision zone between the North China craton and Mongolian arcs and tectonic implications. *Geological Society of America Bulletin* **127**, 1422–36.

Eizenhöfer, P. R., Zhao, G. C., Zhang, J., Han, Y. G., Hou, W. Z., Liu, D. X. & Wang, B. 2015b. Geochemical characteristics of the Permian basins and their provenances across the Solonker Suture Zone: assessment of net crustal growth during the closure of the Palaeo-Asian Ocean. *Lithos* **224**, 240–55.

Eizenhöfer, P. R., Zhao, G. C., Zhang, J. & Sun, M. 2014. Final closure of the Paleo-Asian Ocean along the Solonker Suture Zone: constraints from geochronological and geochemical data of Permian volcanic and sedimentary rocks. *Tectonics* **33**, 441–63.

Faure, M., Lin, W. & Chen, Y. 2012. Is the Jurassic (Yanshanian) intraplate tectonics of North China due to westward indentation of the North China block? *Terra Nova* **24**, 456–66.

Faure, M., Trap, P., Lin, W., Monie, P. & Bruguier, O. 2007. Polyorogenic evolution of the Paleoproterozoic Trans-North China Belt, new insights in Lüliangshan-Hengshan-Wutaishan and Fuping massifs. *Episodes* **30**, 96–107.

Feng, L. X., Brown, R. W., Han, B. F., Wang, Z. Z., Łuszczak, K., Liu, B., Zhang, Z. C. & Ji, J. Q. 2017. Thrusting and exhumation of the southern Mongolian Plateau: joint thermochronological constraints from the Langshan Mountains, western Inner Mongolia, China. *Journal of Asian Earth Sciences* **144**, 287–302.

Gao, H. L. 2010. *Structure evolution and chronology constraints of Langshan in Neimeng Autonomous Region*. Master's thesis, China University of Geosciences, Beijing, China. 70 pp. (in Chinese with English Abstract). Published thesis.

Geisler, T., Schaltegger, U. & Tomaschek, F. 2007. Re-equilibration of zircon in aqueous fluids and melts. *Elements* **3**, 43–50.

Gurnis, M., Hall, C. & Lavier, L. 2004. Evolving force balance during incipient subduction. *Geochemistry, Geophysics, Geosystems* **5**, Q07001. doi: 10.1029/2003GC000681.

Hall, C. E., Gurnis, M., Sdrolias, M., Lavier, L. L. & Müller, R. 2003. Catastrophic initiation of subduction following forced convergence across fracture zones. *Earth and Planetary Science Letters* **212**, 15–30.

Han, J., Zhou, J. B., Wang, B. & Cao, J. L. 2015. The final collision of the CAOB: constraint from the zircon U–Pb dating of the Linxi Formation, Inner Mongolia. *Geoscience Frontiers* **6**, 211–5.

Hoskin, P. W. 2005. Trace-element composition of hydrothermal zircon and the alteration of Hadean zircon from the Jack Hills, Australia. *Geochimica et Cosmochimica Acta* **69**, 637–48.

Hu, J., Gong, W., Wu, S., Liu, Y. & Liu, S. 2014. LA-ICP-MS zircon U–Pb dating of the Langshan Group in the northeast margin of the Alxa Block, with tectonic implications. *Precambrian Research* **255**, 756–70.

Huang, X. F., Shi, W., Chen, P. & Li, H. Q. 2015. Superposed deformation in the Helanshan Structural Belt: implications for Mesozoic intracontinental deformation of the North China Plate. *Journal of Asian Earth Sciences* **144**, 140–54.

Jahn, B. M. 2004. The Central Asian Orogenic Belt and growth of the continental crust in the Phanerozoic. In *Aspects of the Tectonic Evolution of China* (eds J. Malpas, C. J. N. Fletcher, J. R. Ali & J. C. Aitchison), pp. 73–100. Geological Society of London, Special Publication no. 226.

Jian, P., Liu, D. Y., Kröner, A., Windley, B. F., Shi, Y. R., Zhang, F. Q., Shi, G. H., Miao, L. C., Zhang, W., Zhang, Q., Zhang, L. Q. & Ren, J. S. 2008. Time scale of an early to mid-Paleozoic orogenic cycle of the long-lived Central Asian Orogenic Belt, Inner Mongolia of China: implications for continental growth. *Lithos* **101**, 233–59.

Jian, P., Liu, D. Y., Kroner, A., Windley, B. F., Shi, Y. R., Zhang, W., Zhang, F. Q., Miao, L. C., Zhang, L. Q. & Tomurhuu, D. 2010. Evolution of a Permian intraoceanic arc–trench system in the Solonker suture zone, Central Asian Orogenic Belt, China and Mongolia. *Lithos* **118**, 169–90.

Kusky, T. M. & Li, J. H. 2003. Paleoproterozoic tectonic evolution of the North China Craton. *Journal of Asian Earth Sciences* **22**, 383–97.

Kusky, T. M., Windley, B. & Zhai, M. 2007. Tectonic evolution of the North China Block: from orogen to craton to orogen. In *Mesozoic Sub-Continental Lithospheric Thinning Under Eastern Asia* (eds M. Zhai, B. Windley, T. Kusky & Q. Meng), pp. 1–34. Geological Society of London, Special Publication no. 280.

Lawrie, K., Mernagh, T. P., Ryan, C. G., van Achterbergh, E. & Black, L. P. 2007. Chemical fingerprinting of hydrothermal zircons: an example from the Gidginbung high sulphidation Au–Ag–(Cu) deposit, New South Wales, Australia. *Proceedings of the Geologists' Association* **118**, 37–46.

Li, Y. L., Brouwer, F. M., Xiao, W. J., Wang, K. L., Lee, Y. H., Luo, B. J., Su, Y. P. & Zheng, J. P. 2017a. Subduction-related metasomatic mantle source in the

eastern Central Asian Orogenic Belt: evidence from amphibolites in the Xilingol Complex, Inner Mongolia, China. *Gondwana Research* **43**, 193–212.

Li, Y. L., Brouwer, F. M., Xiao, W. J. & Zheng, J. P. 2017b. A Paleozoic fore-arc complex in the eastern Central Asian Orogenic Belt: petrology, geochemistry and zircon U–Pb–Hf isotopic composition of paragneisses from the Xilingol Complex in Inner Mongolia, China. *Gondwana Research* **47**, 323–41.

Li, Y. L., Brouwer, F. M., Xiao, W. J. & Zheng, J. P. 2017c. Late Devonian to Early Carboniferous arc-related magmatism in the Baolidao arc, Inner Mongolia, China: significance for southward accretion of the eastern Central Asian Orogenic Belt. *Geological Society of America Bulletin* **129**, 677–97.

Li, K., Jolivet, M., Zhang, Z. C., Li, J. F. & Tang, W. H. 2016. Long-term exhumation history of the Inner Mongolian Plateau constrained by apatite fission track analysis. *Tectonophysics* **666**, 121–33.

Li, Y. L., Zhou, H. W., Brouwer, F. M., Xiao, W. J., Wijbrans, J. R. & Zhong, Z. Q. 2014. Early Paleozoic to Middle Triassic bivergent accretion in the Central Asian Orogenic Belt: insights from zircon U–Pb dating of ductile shear zones in central Inner Mongolia, China. *Lithos* **205**, 84–111.

Lin, W., Faure, M., Nomade, S., Shang, Q. H. & Renne, P. R. 2008. Permian–Triassic amalgamation of Asia: insight from Northeast China sutures and their place in the final collision of North China and Siberia. *Comptes Rendus Geoscience* **340**, 190–201.

Lin, J., Liu, Y. S., Chen, H. H., Zhou, L., Hu, Z. C. & Gao, S. 2015. Review of high-precision Sr isotope analyses of low-Sr geological samples. *Journal of Earth Science* **26**, 763–74.

Liu, Y. S., Hu, Z. C., Gao, S., Günther, D., Xu, J., Gao, C. G. & Chen, H. H. 2008. In situ analysis of major and trace elements of anhydrous minerals by LA-ICP-MS without applying an internal standard. *Chemical Geology* **257**, 34–43.

Liu, Y. J., Li, W. M., Feng, Z. Q., Wen, Q. B., Neubauer, F. & Liang, C. Y. 2016. A review of the Paleozoic tectonics in the eastern part of Central Asian Orogenic Belt. *Gondwana Research* **43**, 123–48.

Liu, Q., Zhao, G. C., Han, Y. G., Eizenhöfer, P. R., Zhu, Y. L., Hou, W. Z. & Zhang, X. R. 2017. Timing of the final closure of the Paleo-Asian Ocean in the Alxa Terrane: constraints from geochronology and geochemistry of Late Carboniferous to Permian gabbros and diorites. *Lithos* **274–275**, 19–30.

Luo, Z. W., Xu, B., Shi, G. Z., Zhao, P., Faure, M. & Chen, Y. 2016. Solonker ophiolite in Inner Mongolia, China: a late Permian continental margin-type ophiolite. *Lithos* **261**, 72–91.

McNaughton, N. J., Mueller, A. G. & Groves, D. I. 2005. The age of the giant Golden Mile Deposit, Kalgoorlie, Western Australia: ion-microprobe zircon and monazite U–Pb geochronology of a synmineralization lamprophyre dike. *Economic Geology* **100**, 1427–40.

Meng, Q. R., Wei, H. H., Wu, G. L. & Duan, L. 2014. Early Mesozoic tectonic settings of the northern North China craton. *Tectonophysics* **611**, 155–66.

Mossakovsky, A. A., Ruzhentsev, S. V., Samygin, S. G. & Kheraskova, T. N. 1993. The Central Asian fold belt: geodynamic evolution and formation history. *Geotectonics* **26**, 455–73.

Nei Mongol Bureau of Geology and Mineral Resources (NMBGMR). 1991. *Regional Geology of Nei Mongol Autonomous Region*. Beijing: Geological Publishing House.

Park, C., Song, Y., Chung, D., Kang, I. M., Khulganakhuu, M. C. & Yi, K. 2016. Recrystallization and hydrothermal growth of high U–Th zircon in the Weondong deposit, Korea: record of post-magmatic alteration. *Lithos* **260**, 268–85.

Pelleter, E., Cheilletz, A., Gasquet, D., Mouttaqi, A., Annich, M., El Hakour, A., Deloule, E. & Féraud, G. 2007. Hydrothermal zircons: a tool for ion microprobe U–Pb dating of gold mineralization (Tamlalt-Menhouhou gold deposit—Morocco). *Chemical Geology* **245**, 135–61.

Ramsay, J. G. & Huber, M. 1987. Session 21: Strain and small scale structures in folds. In *The Techniques of Modern Structural Geology, Vol. 2 Folds and Fractures*, pp. 445–73. London: Academic Press.

Schaltegger, U. 2007. Hydrothermal zircon. *Elements* **3**, 51–79.

Sengör, A. M. C., Natal'in, B. A. & Burtman, V. S. 1993. Evolution of the Altaid tectonic collage and Paleozoic crustal growth in Eurasia. *Nature* **364**, 299–307.

Shi, G. Z. 2013. *Polycyclic evolution of the Eastern Central Asia Orogenic Belt: microtectonic analysis, geochronology and tectonics in Central Inner Mongolia*. Ph.D. thesis, Université d'Orléans, France. Published thesis.

Shi, G. Z., Faure, M., Xu, B., Zhao, P., Chen, Y. 2013. Structural and kinematic analysis of the Early Paleozoic Ondor Sum-Hongqi mélange belt, eastern part of the Altaids (CAOB) in Inner Mongolia, China. *Journal Asian Earth Science* **66**, 123–39.

Shao, J. A., Tang, K. D. & He, G. Q. 2014. Early Permian tectono-palaeogeographic reconstruction of Inner Mongolia, China. *Acta Petrologica Sinica* **30**, 1858–66 (in Chinese with English abstract).

Song, S., Wang, M. M., Xu, X., Wang, C., Niu, Y., Allen, M. B. & Su, L. 2015. Ophiolites in the Xing'an-Inner Mongolia accretionary belt of the CAOB: implications for two cycles of seafloor spreading and accretionary orogenic events. *Tectonics* **34**, doi: 10.1002/2015TC003948.

Wang, Z. Z., Han, B. F., Feng, L. X. & Liu, B. 2015. Geochronology, geochemistry and origins of the Paleozoic–Triassic plutons in the Langshan area, western Inner Mongolia, China. *Journal of Asian Earth Sciences* **97**, 337–51.

Wang, Z. Z., Han, B. F., Feng, L. X., Liu, B., Zheng, B. & Kong, L. J. 2016. Tectonic attribution of the Langshan area in western Inner Mongolia and implications for the Neoarchean–Paleoproterozoic evolution of the Western North China Craton: evidence from LA-ICP-MS zircon U–Pb dating of the Langshan basement. *Lithos* **261**, 278–95.

Wang, Q. & Liu, X. Y. 1986. Paleoplate tectonics between Cathaysia and Angaraland in Inner Mongolia of China. *Tectonics* **5**, 1073–88.

Wang, C. Y., Wang, P. & Li, W. G. 2004. Conodonts from the Permian Jisu Honguer (Zhesi) Formation of Inner Mongolia, China. *Geobios* **37**, 471–80.

Wang, X. C., Wilde, S. A., Xu, B. & Pang, C. J. 2016. Origin of arc-like continental basalts: implications for deep-Earth fluid cycling and tectonic discrimination. *Lithos* **261**, 5–45.

Wang, Y., Zhou, L. Y. & Li, J. Y. 2011. Intracontinental superimposed tectonics – a case study in the Western Hills of Beijing, eastern China. *Geological Society of America Bulletin* **123**, 1033–55.

https://doi.org/10.1017/S0016756818000183 Published online by Cambridge University Press

Wang, Y., Zhou, L. Y. & Zhao, L. J. 2013. Cratonic reactivation and orogeny: an example from the northern margin of the North China Craton. *Gondwana Research* **24**, 1203–22.

Webb, L. E., Johnson, C. L. & Minjin, C. 2010. Late Triassic sinistral shear in the East Gobi Fault Zone, Mongolia. *Tectonophysics* **495**, 246–55.

Windley, B. F., Alexeiev, D. V., Xiao, W., Kröner, A. & Badarch, G. 2007. Tectonic models for accretion of the Central Asian Orogenic Belt. *Journal of the Geological Society, London* **164**, 31–47.

Xiao, W. J., Windley, B. F., Hao, J. & Zhai, M. G. 2003. Accretion leading to collision and the Permian Solonker suture, Inner Mongolia, China: termination of the central Asian orogenic belt. *Tectonics* **22**, 1069.

Xiao, W. J., Windley, B. F., Huang, B. C., Han, C. M., Yuan, C., Chen, H. L., Sun, M., Sun, S. & Li, J. L. 2009. End-Permian to mid-Triassic termination of the accretionary processes of the southern Altaids: implications for the geodynamic evolution, Phanerozoic continental growth, and metallogeny of Central Asia. *International Journal of Earth Sciences* **98**, 1189–217.

Xiao, W. J., Windley, B. F., Sun, S., Li, J. L., Huang, B. C., Han, C. M., Yuan, C., Sun, M. & Chen, H. L. 2015. A tale of amalgamation of three Permo-Triassic collage systems in Central Asia: oroclines, sutures, and terminal accretion. *Annual Review of Earth and Planetary Sciences* **43**, 477–507.

Xu, B., Charvet, J., Chen, Y., Zhao, P. & Shi, G. Z. 2013. Middle Paleozoic convergent orogenic belts in western Inner Mongolia (China): framework, kinematics, geochronology and implications for tectonic evolution of the Central Asian Orogenic Belt. *Gondwana Research* **23**, 1342–64.

Xu, B., Xu, Y., Li, J. & Li, Q. S. 2016. Age of the Ondor Sum Group in western Inner Mongolia and its position in the Central Asia Orogenic Belt. *Earth Science Frontiers* **23**, 120–7.

Zhang, J., Li, J. Y., Li, Y. F., Qi, W. H. & Zhang, Y. P. 2014. Mesozoic–Cenozoic multi-stage intraplate deformation events in the Langshan Region and their tectonic implications. *Acta Geologica Sinica* (English edition) **88**, 78–102.

Zhang, J., Li, J. Y., Xiao, W. X., Wang, Y. N. & Qi, W. H. 2013. Kinematics and geochronology of multistage ductile deformation along the eastern Alxa block, NW China: new constraints on the relationship between the North China Plate and the Alxa block. *Journal of Structural Geology* **57**, 38–57.

Zhang, J. R., Wei, C. J. & Chu, H. 2015. Blueschist metamorphism and its tectonic implication of Late Paleozoic–Early Mesozoic metabasites in the mélange zones, central Inner Mongolia, China. *Journal of Asian Earth Sciences* **97**, 352–64.

Zhang, J. R., Wei, C. J., Chu, H. & Chen, Y. P. 2016. Mesozoic metamorphism and its tectonic implication along the Solonker suture zone in central Inner Mongolia, China. *Lithos* **261**, 262–77.

Zhang, X. H., Zhang, H. F., Tang, Y. J., Wilde, S. A. & Hu, Z. C. 2008. Geochemistry of Permian bimodal volcanic rocks from central Inner Mongolia, North China: implication for tectonic setting and Phanerozoic continental growth in Central Asian Orogenic Belt. *Chemical Geology* **249**, 262–81.

Zhang, S.-H., Zhao, Y., Kröner, A., Liu, X.-M., Xie, L.-W. & Chen, F.-K. 2009a. Early Permian plutons from the northern North China Block: constraints on continental arc evolution and convergent margin magmatism related to the Central Asian Orogenic Belt. *International Journal of Earth Sciences* **98**, 1441–67.

Zhang, S.-H., Zhao, Y., Song, B., Hu, J.-M., Liu, S.-W., Yang, Y.-H., Chen, F.-K., Liu, X.-M. & Liu, J. 2009b. Contrasting Late Carboniferous and Late Permian–Middle Triassic intrusive belts from the northern margin of the North China block: geochronology, petrogenesis and tectonic implications. *Geological Society of America Bulletin* **120**, 181–200.

Zhang, S.-H., Zhao, Y., Ye, H., Liu, J. M. & Hu, C. Z. 2014. Origin and evolution of the Bainaimiao arc belt: implications for crustal growth in the Southern Central Asian Orogenic Belt. *Geological Society of America Bulletin* **126**, 1275–300.

Zhao, G., Sun, M. & Wilde, S. 2005. Late Archean to Paleoproterozoic evolution of the North China Craton: key issues revisited. *Precambrian Research* **136**, 177–200.

Zhou, Y. Z., Han, B. F., Zhang, B., Xu, Z., Ren, R., Li, X. W. & Su, L. 2013. The Yingba shear zone on the Sino-Mongolian border: southwestern extension of the Zuunbayan Fault from Mongolia to China and implications for Late Mesozoic intracontinental extension in Eastern Asia. *Tectonophysics* **574–575**, 118–32.

Zhu, G., Liu, G., Niu, M., Xie, C., Wang, Y. & Xiang, B. 2009. Syn-collisional transform faulting of the Tan-Lu fault zone, East China. *International Journal of Earth Sciences* **98**, 135–55.

Zhu, G., Wang, Y., Liu, G., Niu, M., Xie, C. & Li, C. 2005. $^{40}Ar/^{39}Ar$ dating of strike-slip motion on the Tan–Lu fault zone, East China. *Journal of Structural Geology* **27**, 1379–98.

Zhu, M. T., Zhang, L. C., Dai, Y. P., Wang, C. L. & Peng, Z. D. 2017. Hydrothermal modification of zircon geochemistry and Lu–Hf isotopes from the Hongtoushan Cu–Zn deposit, China. *Ore Geology Reviews* **86**, 707–18.